IEEE Access
Multidisciplinary | Rapid Review | Open Access Journal

Received 18 September 2022, accepted 13 October 2022, date of publication 19 October 2022, date of current version 27 October 2022.

Digital Object Identifier 10.1109/ACCESS.2022.3216212

RESEARCH ARTICLE

Enhancement the Frequency Stability and Protection of Interconnected Microgrid Systems Using Advanced Hybrid Fractional Order Controller

EMAD A. MOHAMED[1], MOKHTAR ALY[2], (Senior Member, IEEE), AHMED ELMELEGI[1], EMAD M. AHMED[3,4], (Senior Member, IEEE), MASAYUKI WATANABE[5], (Member, IEEE), AND SAYED M. SAID[1]

[1]Department of Electrical Engineering, Faculty of Engineering, Aswan University, Aswan 81542, Egypt
[2]Facultad de Ingeniería, Arquitectura y Diseño, Universidad San Sebastián, Santiago 8420524, Chile
[3]Department of Electrical Engineering, Jouf University, Sakaka 72388, Saudi Arabia
[4]Department of Electrical Engineering, AWCRC, Aswan University, Aswan 81542, Egypt
[5]Department of Electrical and Electronic Engineering, Kyushu Institute of Technology, Kitakyushu, Fukuoka 804-8550, Japan

Corresponding author: Emad A. Mohamed (emad.younis@aswu.edu.eg)

This work was supported in part by JSPS KAKENHI under Grant JP21K04025.

ABSTRACT Substituting conventional energy sources with new renewable sources is crucial issue nowadays in energy generation systems to face climate changes and increased load demands. Due to the increased penetration levels of renewable sources in power systems, the benefits of the high-inertia of conventional sources are being insufficient. The resulting low-inertia power systems introduce several stability, reliability, and coordination problems for power system operation and control. Therefore, this paper tackles the coordination assessment and enhancement between digital frequency relays using a new fractional order load frequency controller equipped with superconducting magnetic energy storage (SMES) virtual inertia system. The improved coordination method is established using optimized fractional order controller based on slime mould optimization algorithm (SMA). The proposed SMA-based design method benefits the adaptive weights of SMA algorithm. The proposed design is generalized to be applied on single area and multi-area interconnected power systems as well. Compared to existing literature, this paper presents an advanced fractional order controller with coordinated operation with existing protection relays. The obtained results show the coordination shortcomings of renewable energy based microgrids with traditional control systems. However, improved design and coordination are obtained using the proposed SMA-optimized fractional order controllers. The superiority and feasibility of the proposed analysis and methods are verified on different case studies using single and multiple interconnected areas.

INDEX TERMS Coordination, digital frequency relay, fraction order control, load frequency controllers, slime mould algorithm (SMA), renewable energy microgrids.

I. INTRODUCTION

Recently, modern power systems and microgrid (MG) systems have become more complex due to the higher existing loads and the higher contribution of renewable energy sources (RESs) [1]. The main driving reasons behind RESs increased penetrations are the economical benefits of RESs, environmental benefits, their availability, etc. The traditional fossil fuel-based power systems have suffered for decades from continuous price increase of fossil fuels, and wider concerns of global warming issues. The wind and photovoltaic (PV) generation systems are the widely installed RESs nowadays [2].

The associate editor coordinating the review of this manuscript and approving it for publication was Youngjin Kim.

The literature has proven that RESs replacements of traditional generation sources can lower the costs of operation and reduce environmental pollution [3]. However, RESs are based on using power electronics converters, which lack the systems' inertia compared to synchronous generations utilized in fossil fuel-based generations. Thence, reduced inertia results in modern power systems and MGs due to their reliance on RESs with high levels of penetration. The reduced inertia is reflected as reduced system's stability, higher frequency deviations, and higher tie-line power fluctuations [4].

Another issue of reduced power system inertia is their coordination and effects on existing digital frequency relays [5]. Modern MGs and power systems have higher peak values of overshoot (OS)/undershoot (US) in addition to longer settling time (ST). Thence, there are additional challenges related to (DFR) coordination with frequency regulation systems at increased penetrations of RESs and higher expected load variations. The availability, reliability, stability, and security of modern MG and power systems are accordingly-affected and further improvements in control design and coordination are needed.

A. LITERATURE REVIEW

The load frequency control (LFC) has been introduced as an effective solution for balancing the load demands and generations during transients. The LFC is a key factor in preserving frequency fluctuations of each connected area and tie-line power deviations at minimized values [6]. several structures of power systems are considered with LFC, such as single area, multiple interconnected areas, nonlinear power system considerations, deregulated power grids, etc. [7]. In which, several control schemes from traditional to advanced ones have been proposed for LFC in the literature [8]. The widely-presented LFC schemes are integer order (IO) controls [7], fractional order (FO) controls [2], model predictive controls (MPCs) [9], artificial intelligence (AI) controls [10], fuzzy logic (FL) controls [11], deep learning controls [3], etc. Several papers have been introduced for reviewing, comparing, and investigating the performance of various LFC schemes [12], [13].

The simple, and suitability to be implemented using cheep microcontrollers properties have lead to wide concentration on traditional IO based PI, and PID controllers [14], [15], [16]. However, tuning processes based on trial-and-error methods require long time for the parameters adjustments. Therefore, great efforts are made by researchers for properly adjusting the control parameters of IO based PI and PID control methods [7]. Among various widely-employed design methodologies for LFC applications, optimization algorithms based tuning schemes have shown improved performance and easier tuning processes [17].

From another side, the FO based LFC schemes have proven better performance compared to IO based LFC. Several FO control structures have been proposed in the literature [8], [18]. Their wide expansion is due that they are flexible and have wider freedom in their tuning. The FOPI, and FOPID have been presented for single and multiple area in several articles [19]. The tilt FO version (TID) has been widely presented for LFC to get over LFC difficulties [1], [20]. The TID provides easier tuning process of parameters, higher ratio for disturbance rejecting, and less plant effect. The TID LFC scheme has been proposed as alternative LFC scheme in several research work. Moreover, hybrid FOPID and TID LFC schemes have been presented in the literature for combining their characterstics [8], [17].

Furthermore, cascaded structures of FLC schemes have been presented in the literature [21], [22]. They can provide more efficient performance, and better enhancement of frequency stability. The I-PD FLC has been proposed for two-area power system in [23]. It has provided minimized frequency fluctuations in interconnected areas compared to PID LFC scheme. The I-TD has been proposed in [18] for improving the performance of I-PD LFC scheme. Another PIDD-PD LFC scheme has been presented in [24], which provided better performance than PID, TID, and ID-T LFC schemes.

A major player in the LFC selection and design is the evolutionary optimizations methods through employing them for optimizing various controllers' parameters [25]. Thence, selecting proper optimizer algorithms represents a crucial challenging factor through the LFC design and selection processes [16]. Several meta-heuristic optimizers have been proposed in the literature, including the manta ray foraging algorithm (MRFO) [17], marine predator algorithm [8], grey wolf optimization (GWO) [26], particle swarm optimizer (PSO) [27], hybrid MPSO-GA optimizer [2], ant-lion optimizer (ALO) [22], the equilibrium optimizer (EO) [28], artificial ecosystem algorithm (AEO) [29], the atomic search optimizer (ASO) [30], imperialist competitive optimizer (ICA) [31], etc.

In [32], an optimized PI controller using GWO algorithm has been proposed for managing hydrogen production in RESs-based hybrid power grids. The adaptive coordination of hydrogen production has proven better performance compared to traditional methods. An improved hybrid fractional order-based combination with fractional filter controller and the artificial hummingbird optimization algorithm (AHA) has been presented in [33]. A robust FOPID controller has been presented in [34] for SMES hybrid energy storage systems in EV applications. The FOPID has proven better performance compared with PID, sliding mode, and feedback linearization controllers. However, frequency regulation and coordination with protective relays in the system have not been considered in this method. From another side, virtual inertia support for low inertia microgrids has been presented in [35] using SMES systems. The PSO algorithm has been proposed for optimizing the FOPI SMES controller to enhance the system stability. However, this work lacks for advanced fractional order controllers with proven better performance than the simple FOPID controller. Moreover,

the protection devices' coordination is not achieved in this work.

However, RESs-based power grids and microgrids (MGs) are suffering from increased OS/US and longer STs due to the reduced inertia [36], [37]. This, in turn, affects the operation of existing protection devices, in particular the DFR devices [5]. Load changes, and/or RESs fluctuations may lead to higher number of disconnection times. Thence, the appropriate selection and design processes of LFC scheme play important role in preserving system connection during transients. Few work has been presented in the literature for the coordination between the DFR and LFC in power grids. In [5], the design of the FLC for superconducting magnetic energy storage (SMES) based virtual inertia controller (VIC) for the Egyptian power grid has been presented. The virtual synchronous generator (VSG) for single area power grid has been presented in [38] with studying their effects on digital protection devices. The coordination between DFR and LFC has been studied with presenting optimized PID controller using the moth swarm optimizer algorithm (MSA) in [39] and using PSO algorithm in [40]. However, recent advanced FO based LFC has not been designed and coordinated with DFR devices based on the authors' knowledge.

The slime mould optimization algorithm (SMA) has been recently proposed with achieving improved performance in several applications [41], [42], [43], [44]. It represents an effective, new, and bio-inspired optimizer algorithm [42]. It employs adaptive weights for simulating processes of positive and negative feedbacks production of propagation waves of slime moulds using the bio-oscillator [43], [44]. The optimum path of food conduction is formed by the bio-oscillator and using excellent exploratory abilities and exploitation propensities. The main characteristics behind SMA superiority can be summarized as following [41]:

1) The biological characteristics of SMA optimizer are unique. This, in turn, enables slime moulds of utilizing varieties of food sources simultaneously. Consequently, slime moulds continue dividing biomass components even if they have previously found better food source to simultaneously exploit both sources at higher food qualities.
2) The slime moulds are able to adjust dynamically the search patterns based on the foodstuff provenience qualities. In which, slime moulds use limited food searching region at high quality of food sources. Thence, the search focus is based on the found food sources. Whereas, slime moulds leave low-quality food sources for exploring better alternatives in the searching region.
3) The SMA optimizer benefits the adaptive searching strategy, which is advantageous when there are different food qualities blocks dispersed in the searching region.
4) The SMA represents new optimizer with simple principle, fast speed for convergence, and low complexity.

Based on characterstics and advantages of SMA optimizer, it is selected for optimizing the various studied controllers in the paper.

B. PAPER CONTRIBUTIONS

It has become clear that the reliability, stability, and availability of RESs-based power grids are highly dependant on the type, design, and coordination of LFC with DFR devices. Thence, the main contribution of this paper is summarized as follows:

1) An improved FO-based LFC method cooperated with PI control method for SMES VIC is proposed in this paper. The proposed controller can improve the grid performance during transients with reducing the overshoot/undershoot peaks and settling time. Compared to existing FO-based LFC, the proposed controller merges the advantages of tilt with FOPID control methods. This, in turn, leads to better system transients and disturbance rejection capability of the proposed modified controller.
2) A coordinated operation and design methodology of LFC and DFR is proposed in as well. The proposed method reduces the disconnection times of the low inertia modern power grids. The proposed method enables avoiding the low-inertia related problems of high penetration levels of renewable energy systems.
3) A simultaneous optimization method is proposed for determining the parameters of the proposed controller.
4) Slime mould optimizer algorithm (SMA) is adopted to optimize the proposed controllers for RESs-based power grids. The main benefits of the SMA optimizer are the use of adaptive weights during global optimum parameters searching processes.

The remaining of the paper is organized as following: The operation of DFR and its coordination with LFC is explained in Section II. Section III presents the mathematical representation of the single and multi-area MG systems. Section IV details the proposed FO controller and its coordination strategy with DFR. Moreover, the design optimization process and SMA optimizer are also presented in this section. and with its optimization process. Section V shows the obtained results and discussions using single and two-area MG systems. Paper conclusions are provided in Section VI.

II. COORDINATION BETWEEN LFC AND DFR IN MICROGRIDS

A. DIGITAL FREQUENCY RELAYS (DRFs) IN MICROGRIDS

The DFR is responsible for digitally detecting the operating frequency of MG systems and detect the over/underfrequency conditions to isolate the MG system. The main three stages in DFR system are shown in Fig. 1, which can be described as following:

1) **Sampling:** In this stage, the operating frequency is sampled and discretized using the ADC stage. Thence, measured frequency signal as a continuous time signal

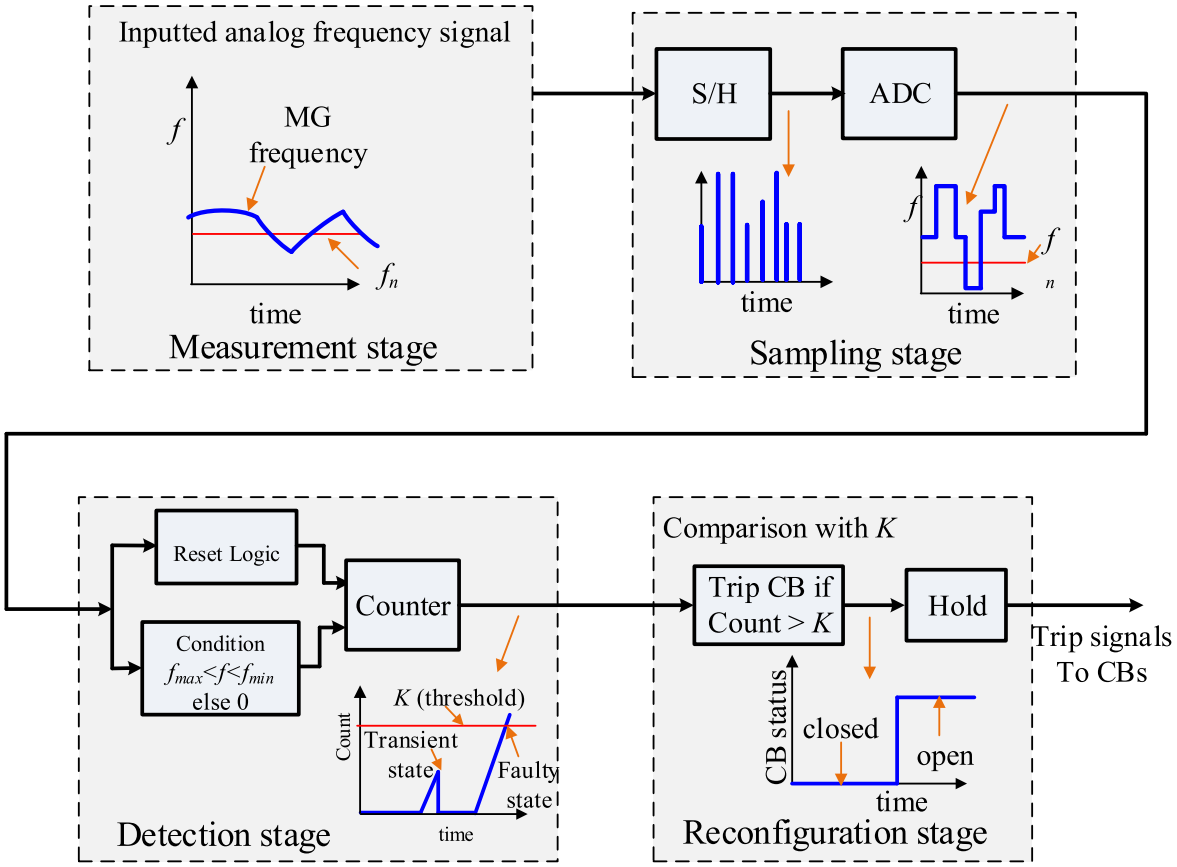

FIGURE 1. Operation and stages of DFR system in MGs.

is outputted from this stage as a sampled digital signal to be used with the DFR.

2) **Detection:** The digital frequency signal is fed into this stage to classify the normal, transient, and abnormal over/underfrequency cases. The inputted frequency signal is compared with an upper limit (f_{max}, which denotes to the maximum operating frequency limit of MG system) and lower limit (f_{min}, which denotes to the minimum operating frequency limit of MG system). The setting of the upper limit f_{max} is adjusted to 51 Hz in the studied MGs, whereas the lower limit f_{min} is adjusted to 49 Hz [5]. The normal condition is detected when the inputted frequency signal lies between the upper and lower limits ($f_{min} < f_g < f_{max}$). To classify between the transient state and the faulty state, a counter of frequency cycles is employed before the disconnection action of the MG system. The counter starts the counting operation in the case of higher measured frequency than f_{max} at the overfrequency faulty scenario. Also, the counter starts the counting operation in the case of lower measured frequency than f_{min} at the underfrequency faulty scenario.
3) **Reconfiguration:** The threshold value is adjusted to classify between the transient and faulty scenarios. In the case that counted cycles outside the limits reach the value of predefined count threshold, the trip signal will be generated to take the reconfiguration and disconnection actions. The MG's relays are energized and tripping signals are sent to circuit breakers when the two conditions happen simultaneously. The selected threshold value of the counter is dependant on the operation of MGs and their transients. In this work, the threshold is set to 20 cycles (1 second) for distinguishing the MG transients with the faulty conditions. The stage of reconfiguration is responsible for taking the appropriate protection and control actions in the MG system. This, in turn, includes disconnection/connection of various connected elements, load shedding/management, etc. The employed DFR is suitable for digital microprocessor implementations with communication systems with various power system components.

B. LFC IN THE LITERATURE

Several control schemes have been proposed in the literature for LFC in single and multi-area MGs. The main objectives for these controllers are mitigating frequency deviations in various areas, and eliminating tie-line power fluctuations between the areas. The TFs between LFC output $Y(s)$ and

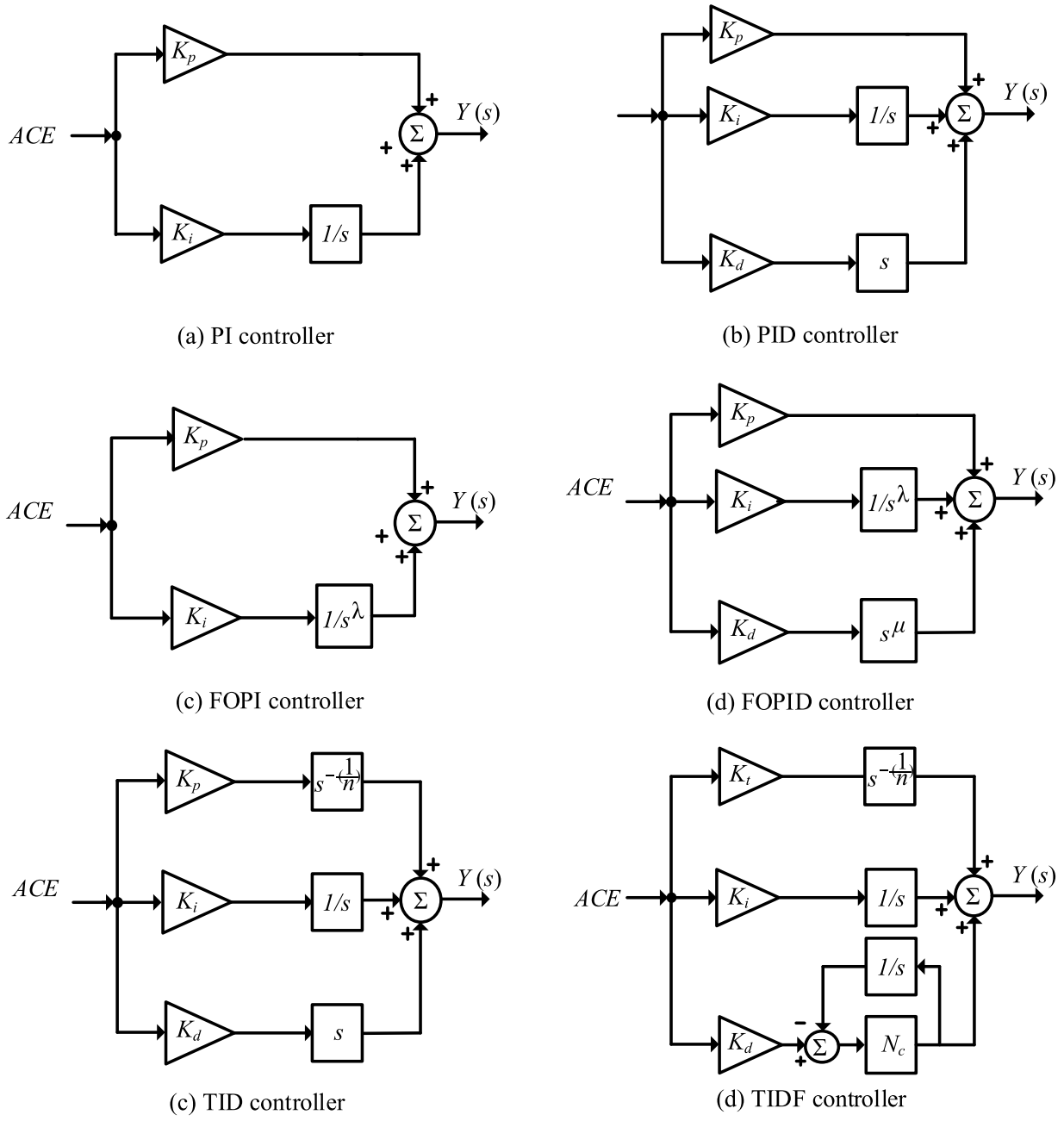

FIGURE 2. Schematics for existing LFC in literature.

controller input $E(s)$ are expressed as following:

$$
\begin{aligned}
C_{PI}(s) &= \frac{Y(s)}{E(s)} = K_p + \frac{K_i}{s} \\
C_{FOPI}(s) &= \frac{Y(s)}{E(s)} = K_p + \frac{K_i}{s^{\lambda}} \\
C_{PID}(s) &= \frac{Y(s)}{E(s)} = K_p + \frac{K_i}{s} + K_d\ s \\
C_{FOPID}(s) &= \frac{Y(s)}{E(s)} = K_p + \frac{K_i}{s^{\lambda}} + K_d\ s^{\mu} \\
C_{TID}(s) &= \frac{Y(s)}{E(s)} = K_t\ s^{-(\frac{1}{n})} + \frac{K_i}{s} + K_d\ s
\end{aligned} \tag{1}
$$

where, $C_{PI}(s)$, $C_{FOPI}(s)$, $C_{PID}(s)$, $C_{FOPID}(s)$, and $TID(s)$ are the TFs of the PI, FOPI, PID, FOPID, and the TID LFC schemes, respectively. In (1), K_p, K_d, and K_i are the proportional, differential, and the integral gains, respectively. Whereas, λ is the integration FO operator, and μ is the differentiation FO operator, and n is the tilt FO operator. Fig. 2 shows the widely-presented LFC schemes in the literature as presented in (1).

C. COORDINATION PROBLEMS

It has become clear from the above-mentioned discussion that the operation of protection and control systems interact

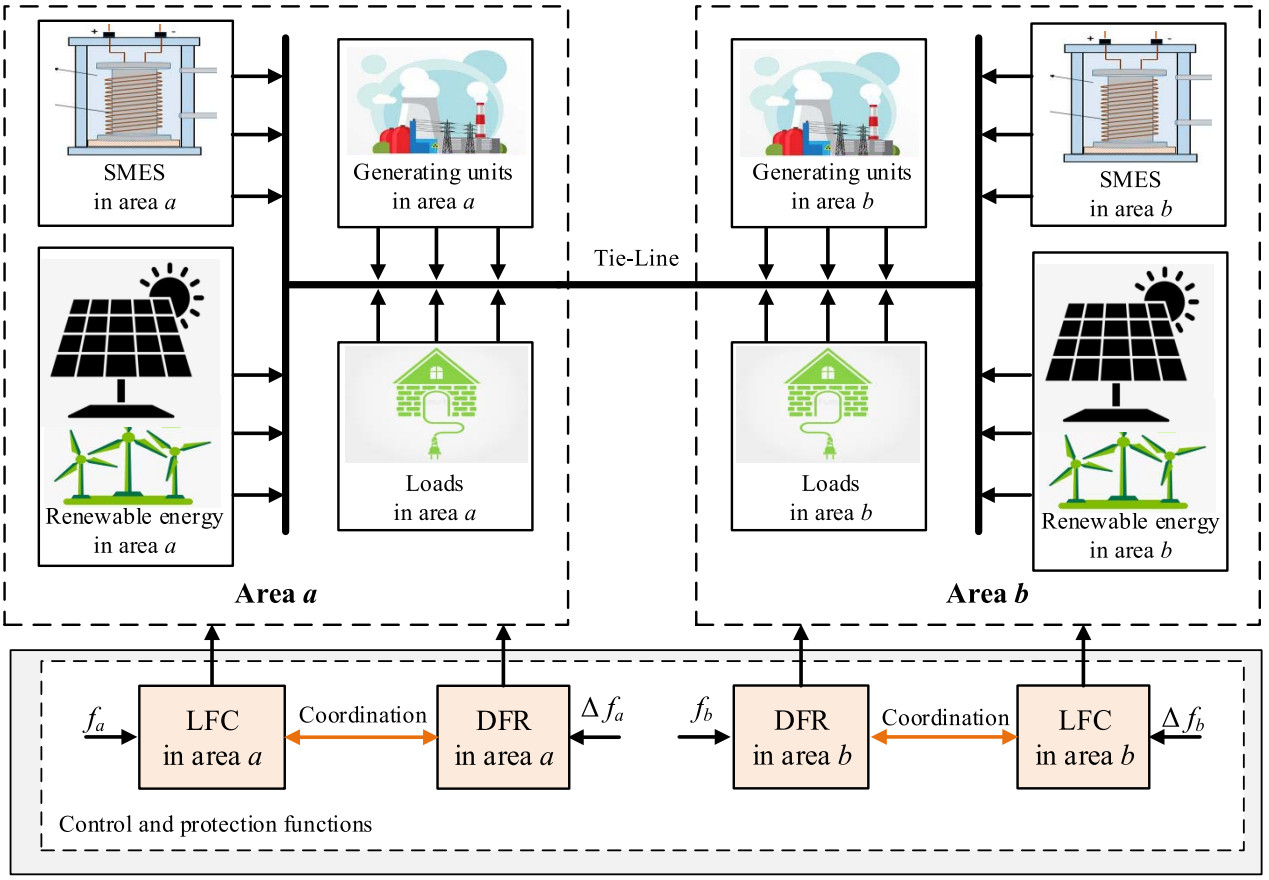

FIGURE 3. General structure of two-area MG with control and protection coordination.

together. The classifications between control operation during transients with the faulty scenarios are essential. The discrimination between transients and faults can lead to fewer times of system disconnection and thence proper utilization of connected renewable energy sources and energy storage devices. The coordination problems can be summarized as following:

- The various control methods have different system responses of frequency deviations, regarding the peak overshoot/undershoot values and their time durations. Thence, proper selection and design of LFC to cope with DFR systems are important task.
- Proper threshold values that represent the transient time is important factor in taking decision of continuing the connection or disconnecting the MG system. It is also depending on the control type and design method.
- Coordination between the design and operation of LFC with DFR settings can lead to improved reliability and availability of MG systems. This, in turn, can achieve better utilization of available renewable energy sources, and improvement of supply reliability for users.
- Recent renewable energy based MGs also suffer from reduced power system inertia, which affects directly the transients of MGs with increasing peak overshoot/undershoot values with their durations. Thence, the design and selection processes of LFC methods have become difficult tasks and improvements are essential.

III. MATHEMATICAL MODELS FOR THE STUDIED MICROGRIDS

A. MODELLING OF MG ELEMENTS

The single and multi-area case studies have been employed for verifying the proposed method and analysis. The complete structure of two area MG system with control and protection coordination is shown in Fig. 3. Fig. 4 shows the model of single area microgrid, whereas the model for two-area power system is shown in Fig. 5. Each MG includes conventional generation (thermal plants), renewable power generation sources (PV and wind), energy storage (SMES), and connected loads. The LFC is responsible for controlling the frequency deviations in the studied MGs in addition to the tie-line power deviations among MGs. Moreover, coordination of the DFR operation with the LFC operation is essential to reduce the blackout scenarios and reduce the peaks during the transients. Additionally, the SMES control and contribution can be managed to support the MG systems during transients and the existing disturbances in the loading and renewable energy generations. Thence, the stability, security, and reliability are highly-affected by the type and design of LFC systems in addition to the DFR operation. In this section,

TABLE 1. Definitions of symbols and their values in the proposed study (where, $x \in \{a, b\}$), [38], [40].

Symbols	Definition	Value	
		area a	area b
P_{rx} (MW)	rated area's capacity	20	20
R_x (Hz/MW)	droop loop constant	2.4	2.4
B_x (MW/Hz)	frequency biased value	0.4249	0.4249
V_{vlx} (p.u.MW)	minimum value of valve gate's limit	-0.3	-0.3
V_{vux} (p.u.MW)	maximum value of valve gate's limit	0.3	0.3
T_g (s)	thermal governor's time constants	0.1	0.1
T_t (s)	thermal turbine's time constants	0.4	0.4
H_x (p.u.s)	power system's inertia constants	0.083	0.083
D_x (p.u./Hz)	power system's damping coefficients	0.015	0.015
T_{PV} (s)	PV's TF time constants	1.8	1.8
K_{PV} (s)	PV TF's gains	1	1
T_{WT} (s)	wind TF's time constants	1.5	1.5
K_{WT} (s)	wind TF's gains	1	1
T_{DCx} (s)	SMES power converter's time constants	0.03	0.03
L_x (H)	SMES coil's inductance	0.03	0.03
K_{SMESx} (kV/unit MW)	SMES side gains	100	100
K_{Idx} (kV/kA)	SMES controller gains	0.2	0.2
I_{d0x} (kA)	SMES inductor's rated currents	4.5	4.5
$P_{SMESmax}$ (pu Mw)	SMES Maximum capacity	+0.3	+0.3
$P_{SMESmin}$ (pu Mw)	SMES Minimum capacity	-0.3	-0.3
A_{ab}	capacity ratios between areas	-1	
$T_{tie,ab}$ (s)	synchronizing coefficients of tie-line	0.0662	

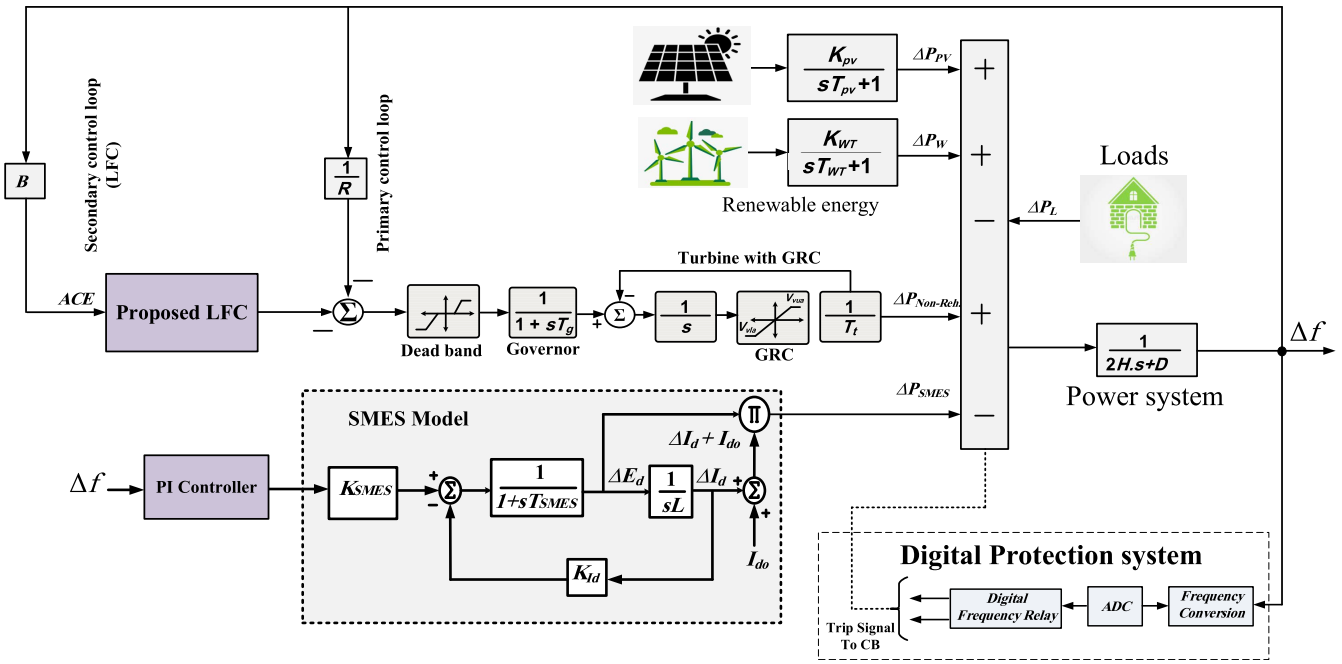

FIGURE 4. Model of single MG system.

the mathematical representations of the studied systems are introduced.

The model transfer function (TF) of thermal power generation (including governor TF $G_{gx}(s)$ and turbine TF $G_{tx}(s)$) is expressed as following [45].

$$G_{gx}(s) = \frac{1}{T_{gx}s + 1} \tag{2}$$

$$G_{tx}(s) = \frac{1}{T_{tx}s + 1} \tag{3}$$

The definitions of various employed symbols in this paper are shown in Table. 1. The MG models of their TFs $G_{px}(s)$ are expressed as following [38], [40]:

$$G_{px}(s) = \frac{1}{2H_x s + D_x} \tag{4}$$

The TFs for renewable power generations (PV $G_{PVx}(s)$ and wind $G_{WTx}(s)$) are expressed as following [46]:

$$G_{PVx}(s) = \frac{K_{PVx}}{T_{PVx}s + 1} \tag{5}$$

$$G_{Wx}(s) = \frac{K_{Wx}}{T_{Wx}s + 1} \tag{6}$$

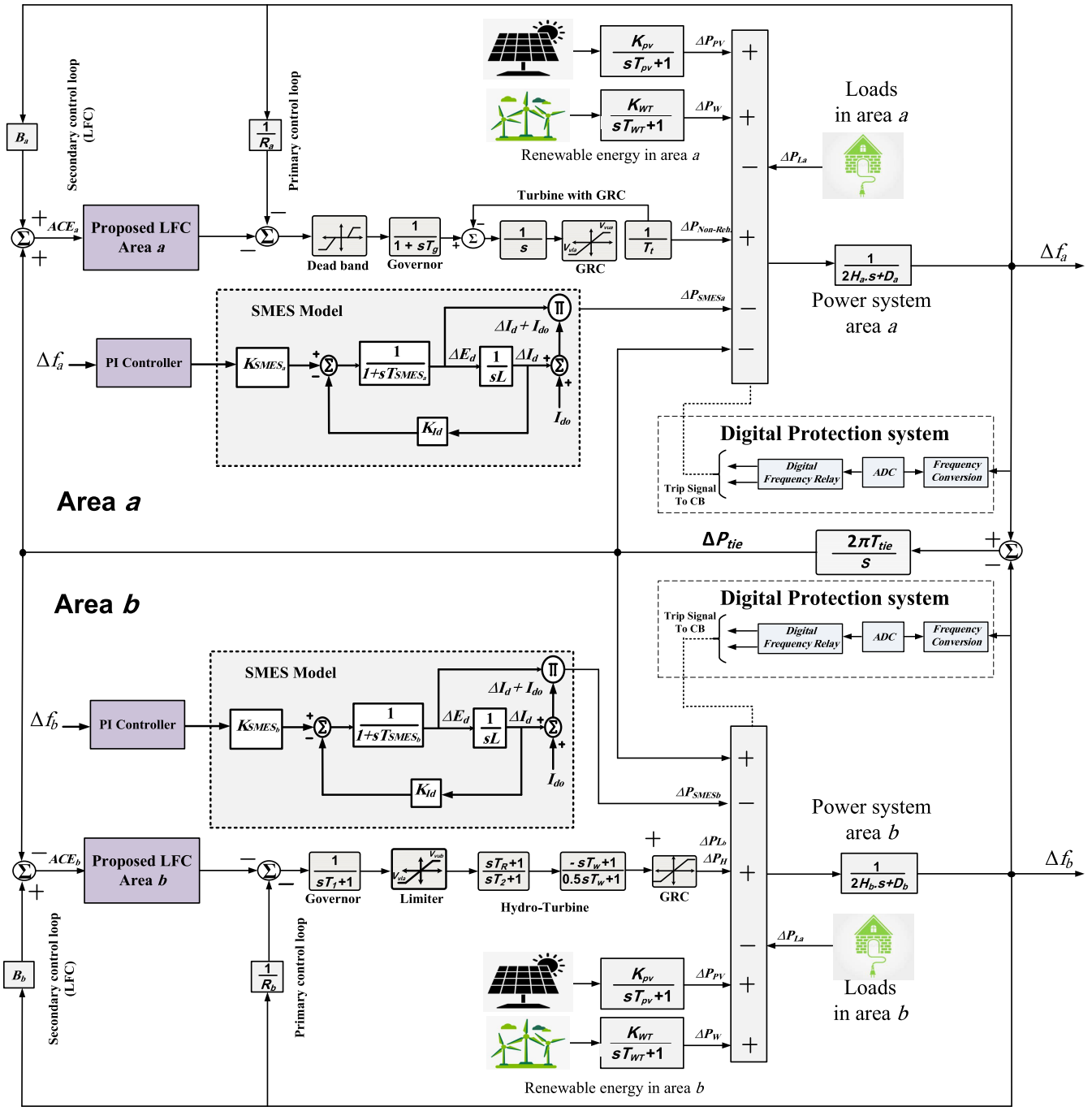

FIGURE 5. Structure and interconnection of two MG systems Model.

B. SMES MODELLING

The practical representation model of SMES is employed in this paper as in [47] and [48]. The utilization of SMES in this study is due to its superiority over the other existing energy storage systems. For frequency regulation, SMES can perfectly mitigate fast frequency deviations due to its faster response, longer lifetime, and higher efficiency [48], [49]. The power conversion system of SMES includes DC-DC converter, DC-link capacitors, voltage source inverter (VSI). The DC-DC converter is responsible for controlling the charging/discharging currents of SMES. Whereas, the VSI is responsible for integrating the SMES system with the MG AC system.

The SMES is charged from the grid at normal operating mode and it becomes ready for compensating the various system fluctuations during abnormalities. When disturbances occur in the MG system, the SMES starts the discharging phase through its power conversion system to restore the

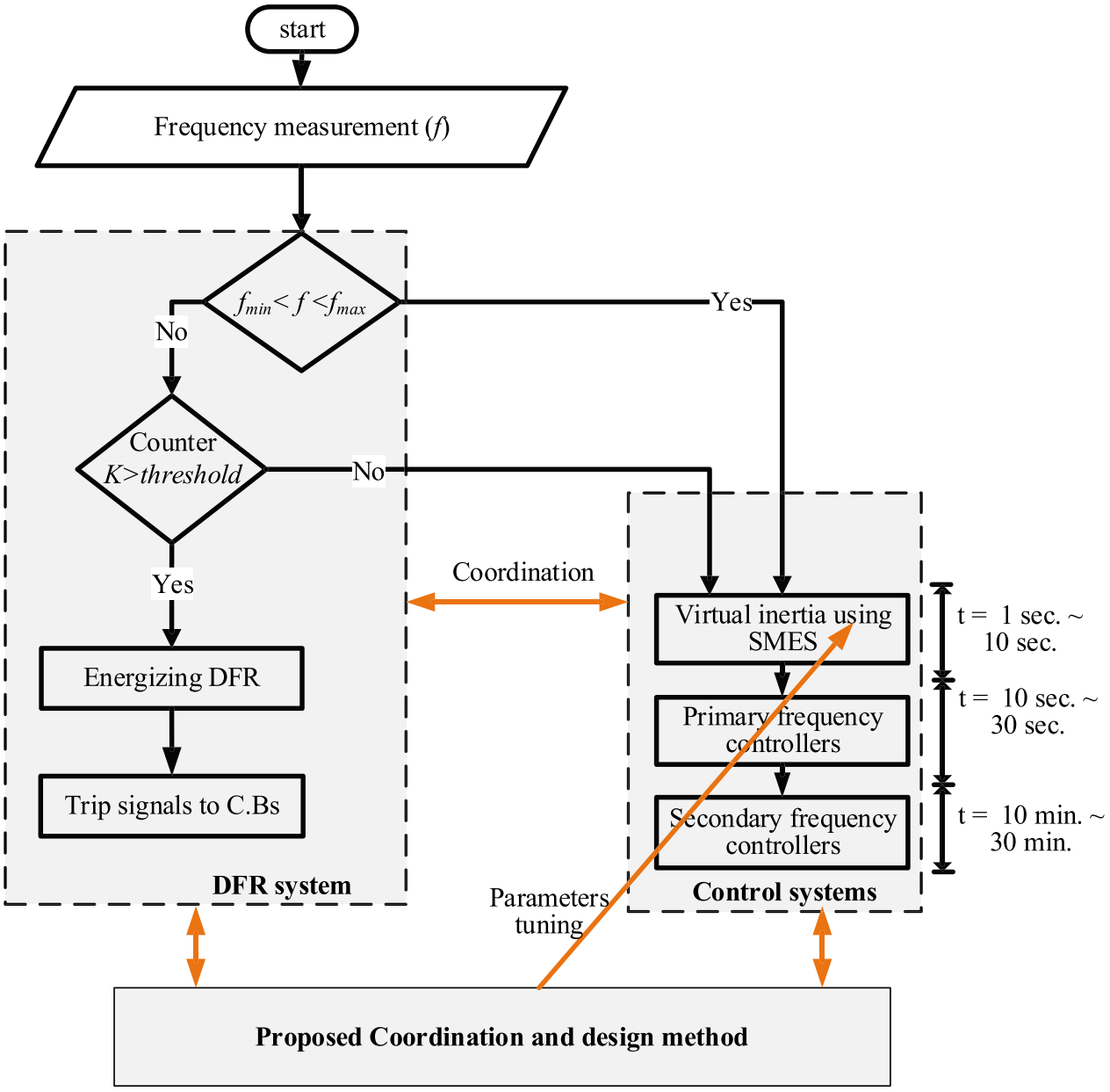

FIGURE 6. Proposed coordination and design method.

equilibrium of MG and maintain system balance [50]. The employed model in this work is based on the linearized first-order MSES model, which is more appropriate for LFC studies. The dynamical model of SMES for LFC is included in the general structure for single area in Fig. 4 and for two-area in Fig. 5

C. MGs COMPLETE STATE SPACE MODELS

The frequency fluctuations in each area (Δf_a and Δf_b) based on Fig. 4 and Fig. 4 are expressed as following:

$$\Delta f_a = \frac{1}{2H_a s + D_a}[\,\Delta P_{ga} + \Delta P_{Wa} + \Delta P_{PVa} - \Delta P_{La} - \Delta P_{SMES_a} - \Delta P_{tie,ab}] \quad (7)$$

$$\Delta f_b = \frac{1}{2H_b s + D_b}[\,\Delta P_{gb} + \Delta P_{Wb} + \Delta P_{PVb} - \Delta P_{Lb} - \Delta P_{SMES_b} + A_{ab}\ \Delta P_{tie,ab}] \quad (8)$$

The study of dynamical performance of the system is achieved through combining the above-mentioned models in complete MG representation. The equations are derived based on the dynamical models of MGs, conventional and renewable generations, loads, and energy storage devices. The state space representation is the widely-utilized model for MGs. The general state-space modelling for single and multi-area MGs is expressed as following:

$$\dot{x} = Ax + B_1\omega + B_2 u$$
$$y = Cx \quad (9)$$

where x, y, ω and u are the system states variables vector, the outputs states vector, disturbances vector, and control variables vector, respectively. Whereas, A, B_1, B_2, and C are their corresponding parameter matrices in the linearized state space representation of the MG system.

For the single area MG, the matrices and vectors are expressed as following:

$$x_a = \left[\Delta f_a \ \Delta P_{ga} \ \Delta P_{ga1} \ \Delta P_{Wa} \ \Delta P_{PVa}\right]^T \tag{10}$$

$$\omega_a = \left[\Delta P_{la} \ P_{Wa} \ P_{PVa}\right]^T \tag{11}$$

$$u_a = \left[ACE_a \ \Delta P_{SMES_a}\right]^T \tag{12}$$

$$A_a = \begin{bmatrix} -\frac{D_a}{2H_a} & \frac{1}{2H_a} & 0 & \frac{1}{2H_a} & 0 \\ 0 & -\frac{1}{T_{ta}} & \frac{1}{T_{ta}} & 0 & 0 \\ -\frac{1}{R_a T_{ga}} & 0 & -\frac{1}{T_{ga}} & 0 & 0 \\ 0 & 0 & 0 & -\frac{1}{T_{Wa}} & 0 \\ 0 & 0 & 0 & 0 & -\frac{1}{T_{PVa}} \end{bmatrix} \tag{13}$$

$$B_{1a} = \begin{bmatrix} -\frac{1}{2H_a} & 0 & 0 \\ 0 & 0 & 0 \\ 0 & 0 & 0 \\ 0 & \frac{K_{Wa}}{T_{Wa}} & 0 \\ 0 & 0 & \frac{K_{PVa}}{T_{PVa}} \end{bmatrix} \tag{14}$$

$$B_{2a} = \begin{bmatrix} 0 & -\frac{1}{2H_a} \\ 0 & 0 \\ -\frac{1}{T_{ga}} & 0 \\ 0 & 0 \\ 0 & 0 \end{bmatrix} \tag{15}$$

$$C_a = \left[B_a \ 0 \ 0 \ 0 \ 0\right] \tag{16}$$

whereas, for two-area MG system, the matrices and vectors are expressed as following:

$$x = \left[x_a \ x_b \ \Delta P_{tie,ab}\right]^T, \quad \omega = \left[\omega_a \ \omega_b\right]^T \tag{17}$$

$$u = \left[u_a \ u_b\right]^T \tag{18}$$

$$A = \left[\begin{array}{cccccccccc|c} & & & & & & & & & & -\frac{1}{2H_a} \\ & & & & & & & & & & 0 \\ & & & A_a & & & & 0_{5\times5} & & & 0 \\ & & & & & & & & & & 0 \\ & & & & & & & & & & 0 \\ \hline & & & & & & & & & & -\frac{1}{2H_a} \\ & & & & & & & & & & 0 \\ & & & 0_{5\times5} & & & & A_b & & & 0 \\ & & & & & & & & & & 0 \\ & & & & & & & & & & 0 \\ \hline 2\pi T_{tie,ab} & 0 & 0 & 0 & 0 & -2\pi T_{tie,ab} & 0 & 0 & 0 & 0 & 0 \end{array}\right] \tag{19}$$

$$B_1 = \left[\begin{array}{ccc|cc} & & & & \\ & B_{1a} & & 0_{5\times3} & \\ & & & & \\ \hline & & & & \\ & 0_{5\times3} & & B_{1b} & \\ & & & & \\ 0 & 0 & 0 & 0 & 0 \ 0 \end{array}\right], \quad \text{and} \quad B_2 = \left[\begin{array}{cc|cc} & & & \\ & & & \\ B_{2a} & & 0_{5\times2} & \\ & & & \\ \hline & & & \\ & & & \\ 0_{5\times2} & & B_{2b} & \\ & & & \\ 0 & 0 & 0 & 0 \end{array}\right] \tag{20}$$

$$C = \begin{bmatrix} 1 & 0 & 0 & 0 & 0 & 0 & 0 & 0 & 0 & 0 \\ B_a & 0 & 0 & 0 & 0 & 0 & 0 & 0 & 0 & 1 \\ 0 & 0 & 0 & 0 & 0 & 1 & 0 & 0 & 0 & 0 \\ 0 & 0 & 0 & 0 & 0 & B_b & 0 & 0 & 0 & -1 \end{bmatrix} \tag{21}$$

IV. THE PROPOSED METHOD FOR ENHANCING COORDINATION BETWEEN LFC AND DFR SYSTEMS

Fig. 6 shows the proposed design and coordination strategy in this paper between the DFR system and various control systems. As explained previously, the DFR is activated in the case that the measured frequency signal exceeds predefined maximum/minimum limits of frequency. Then, a threshold value is adjusted to coordinate between the MG transients and the LFC method, especially at low inertia. Then, reconfiguration strategies are applied and CBs are tripped to disconnect the system at faulty scenarios.

From another side, coordinated control strategies with proper parameters tuning are crucial for more reliable MG systems. Normally, control schemes are operated in three different control levels, including the virtual inertia, primary controller, and secondary controller. Proper management and coordination between the three control stages is required for maintaining system's frequency stability and for reducing disconnection times of MG system.

The control of SMES unit as virtual inertia system is responsible for eliminating fast MG transients between 1 sec. to 10 sec. ranges. The SMES unit represents the first acting stage to achieve the generation and loading balance. Then, primary controller is responsible for stabilizing the MG frequency to the steady-state between 10 sec. to 30 sec. The last control stage is secondary controller that is responsible for recovering the MG frequency to its nominal value between 10 min. to 30 min. In the proposed coordination and control method, the SMES participates in the stabilization of MGs against its disturbances with the proposed LFC method. In the following subsections, detailed description of the new proposed controller and design method with the optimization process will be given.

A. THE PROPOSED CONTROLLER

Fig. 7 shows the two-area MG with the proposed LFC and SMES control. The main target of the proposed control is mitigating frequency and tie-line power fluctuations. In addition, it coordinates the transient response with the DFR system so as to reduce the number of MG's disconnection. The proposed control method is based on combining FO control methods based on the FOPID with the TID, which have proven enhanced performance in LFC. The resulting combined controller contains the tilt branch with the FOID branches from FOPID, namely the FOTID control. The proposed FOTID LFC is coordinated with the classical PI control for SMES system. The design optimization for the LFC and SMES controllers in single/two-area are simultaneously made.

The proposed FOTID control method employs the integral and the derivative FO branches from the FOPID, which improve the MG stability, and MG robustness. In addition, the two utilized branches are advantageous for reducing settling times during disturbance occurrence. Thence, adding the integral and the derivative FO branches enriches the TID control through higher flexibility and freedom instead of integer order based derivative and integral branches. Therefore, the proposed FOTID LFC scheme can combine the best features from the TID and the FOPID LFC schemes. The resulting TF of the FOTID is mathematically expressed as following:

$$C(s) = \frac{Y(s)}{E(s)} = K_t \; s^{-(\frac{1}{n})} + \frac{K_i}{s^{\lambda}} + K_d \; s^{\mu} \tag{22}$$

Proper optimization of FOTID LFC scheme simultaneously with SMES PI control scheme can mitigate the fluctuations during transients in addition to reducing the possibility of the disconnection of MGs. Based on Fig. 7, the FOTID LFC contains six tunable control parameters, whereas the SMES PI controller includes two other tunable parameters. The proper selection and tuning processes of these control parameters are essential to optimize MG performance and reliability. The recently-presented advanced metaheuristic optimizers can be utilized for the simultaneous determination process of optimized control parameters for LFC and SMES in single/two-area systems.

B. THE PROCESS FOR OBTAINING OPTIMIZED CONTROL PARAMETERS

As shown in Fig. 7, the objective function is used in the process of determining optimized values for LFC and PI controllers in single/two-area MGs. The single area MG has total of 8 tunable parameters (6 for FOTID LFC and 2 for SMES PI control. Whereas, the two-area MG has total of 16 tunable ones (8 in each area with 6 for FOTID LFC and 2 for SMES PI control). The widely-employed integral squared error (ISE) objective function is used in this work. It is expressed as following:

$$ISE = \int \sum_{i=1}^{m} (e_i^2) \; \mathrm{d}t \tag{23}$$

In single area MG, the controllers have to reduce the frequency deviation of the area. Thence the error in (23) is represented by Δf_a. Whereas, in two-area MG, the objective is to mitigate frequency deviation in both areas in addition to the tie-line power variations between them. Thence, the error in (23) is represented by Δf_a, Δf_b), and (ΔP_{tie}). The ISE representations can be expressed for single area as following:

$$ISE = \int_0^{t_s} ((\Delta f_a)^2) \; \mathrm{d}t \tag{24}$$

And, for two-area MG, it is expressed as following:

$$ISE = \int_0^{t_s} ((\Delta f_a)^2 + (\Delta f_b)^2 + (\Delta P_{tie})^2) \; \mathrm{d}t \tag{25}$$

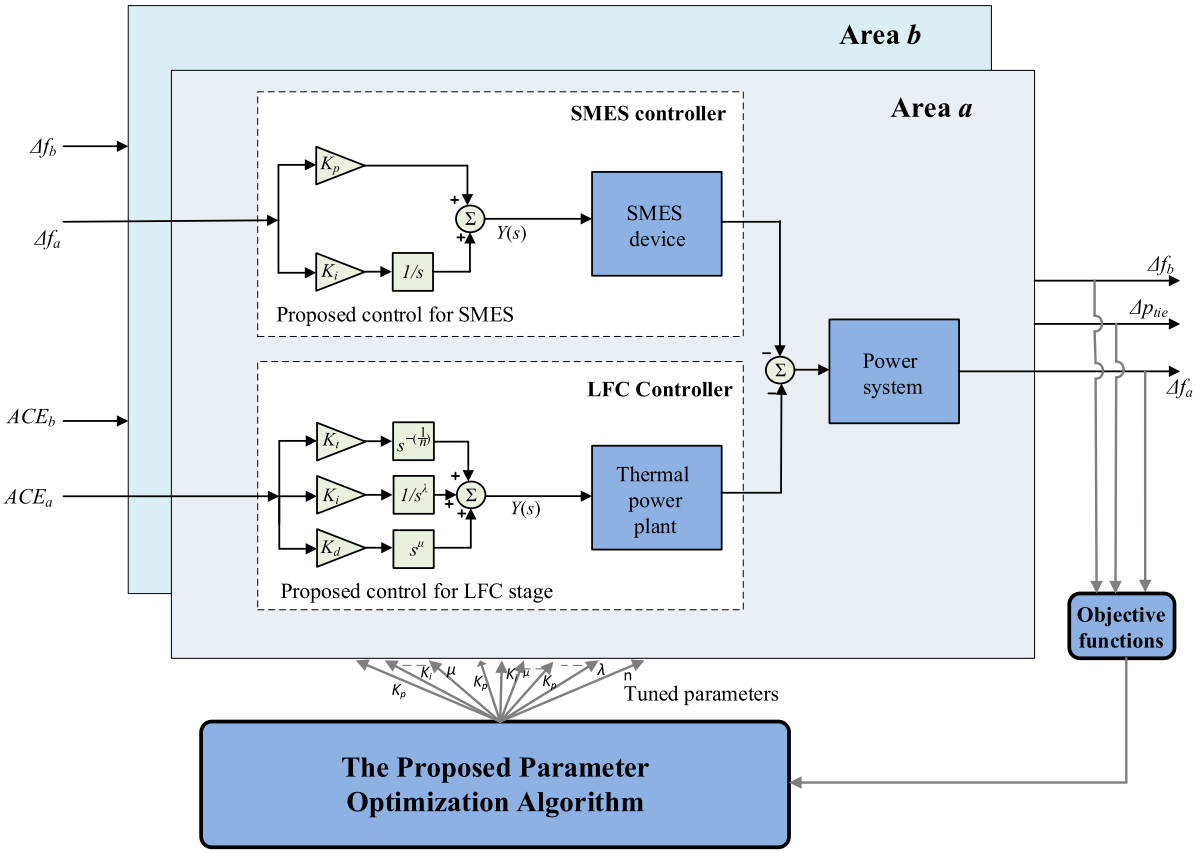

FIGURE 7. Proposed optimized controllers for LFC and SMES devices.

The minimum and maximum values for the tunable control parameters are expressed for single area MG as following:

$$\begin{aligned} K_p^{min} &\le K_p \le K_p^{max} \\ K_t^{min} &\le K_t \le K_t^{max} \\ K_i^{min} &\le K_{i1}, K_{i2} \le K_i^{max} \\ K_d^{min} &\le K_d \le K_d^{max} \\ n^{min} &\le n \le n^{max} \\ \lambda^{min} &\le \lambda \le \lambda^{max} \\ \mu^{min} &\le \mu \le \mu^{max} \end{aligned} \tag{26}$$

whereas, they are expressed for two-area MG as following:

$$\begin{aligned} K_p^{min} &\le K_{p1}, K_{p2} \le K_p^{max} \\ K_t^{min} &\le K_{t1}, K_{t2} \le K_t^{max} \\ K_i^{min} &\le K_{i1}, K_{i2}, K_{i3}, K_{i4} \le K_i^{max} \\ K_d^{min} &\le K_{d1}, K_{d2} \le K_d^{max} \\ n^{min} &\le n_1, n_2 \le n^{max} \\ \lambda^{min} &\le \lambda_1, \lambda_2 \le \lambda^{max} \\ \mu^{min} &\le \mu_1, \mu_2 \le \mu^{max} \end{aligned} \tag{27}$$

where, the limits with $(f)^{min}$ represent the lower limiting bounds, and the limits with $(f)^{max}$ represent the upper limiting bounds of the obtained optimized values for control parameters. The lower limiting bounds for control gains (K_p^{min}, K_t^{min}, K_i^{min}, and K_d^{min}) equal zero, whereas the upper limiting bounds (K_p^{max}, K_t^{max}, K_i^{max}, K_d^{max}) equal 5 in the proposed optimization processes. The lower limiting bound for n (n^{min}) is 2, whereas the upper limiting bound (n^{max}) is 10. The lower limiting bounds for μ, and λ (μ^{min}, and λ^{min}, respectively) are 0, and their upper limiting bounds (μ^{max}, and λ^{max}) are 1 in the proposed optimization processes.

C. THE SLIME MOULD OPTIMIZER ALGORITHM (SMA)

This subsection introduces a short introduction for the SMA optimizer. The concept and mathematical modelling of SMA optimizer is presented in [41], and it has found wide applications with improved performance [42], [43], [44]. SMA optimizer simulates the behavior change of slime moulds at only their foraging without using their complete life-cycle model. The adaptive weights are employed in SMA optimizer for simulating negative and positive feedback, which is generated by slime moulds at their foraging processes, and three different morphotype are created. The approaching behaviors of slime moulds are mathematically represented through imitating concentration mode as following [41]:

$$\overrightarrow{X(t+1)} = \begin{cases} \overrightarrow{X_b(t+1)} + \overrightarrow{vb} \cdot (\overrightarrow{W} \cdot \overrightarrow{X_A(t)} - \overrightarrow{X_B(t)}) & r < p \\ \overrightarrow{vc} \cdot \overrightarrow{X(t)} & r \ge 0 \end{cases} \tag{28}$$

where $\overrightarrow{vb}$ represents parameter within the range $[-a, a]$, $\overrightarrow{vc}$ is linearly decreasing from 1 to 0, t is current iteration, $\overrightarrow{X_b}$ is individual locations with highest currently-found odor concentrations, $\overrightarrow{X}$ is the slime moulds locations, $\overrightarrow{X_A}$ and $\overrightarrow{X_B}$ are two randomly-selected swarm individuals, $\overrightarrow{W}$ is the slime mould's weight. The value of p is modelled as following:

$$p = \tanh|S(i) - DF| \tag{29}$$

where, $i \in \{1, 2, \ldots, n\}$, $S(i)$ is $\overrightarrow{X}$ fitness of, DF is the best-obtained fitness value within the iterations. The value of $\overrightarrow{vb}$ is represented as following:

$$\overrightarrow{vb} = [-a, a] \tag{30}$$

$$a = (-\frac{t}{max\_t} + 1) \tag{31}$$

The formula of $\overrightarrow{W}$ is listed as follows:

$$\overrightarrow{W(sindex(i))} = \begin{cases} 1+r\cdot\log(\frac{bF - S(i)}{bF - wF} + 1), & cond. \\ 1-r\cdot\log(\frac{bF - S(i)}{bF - wF} + 1), & others \end{cases} \tag{32}$$

$$sindex = sort(S) \tag{33}$$

where, the condition shows that $S(i)$ ranks the first half of populations, r denotes to random value within [0, 1] interval, bF denotes to the optimal-obtained fitness within current iterative processes, wF denotes to the worst-obtained fitness with current iterative processes, $SIndex$ denotes to sorted values fitness sequence (ascending in minimized value problem). Mathematical representation of slime moulds locations' update is expressed as following:

$$\overrightarrow{X^*} = \begin{cases} rand \cdot (UB - LB) + LB, & rand < z \\ \overrightarrow{X_b(t)} + \overrightarrow{vb} \cdot (W \cdot \overrightarrow{X_A(t)} - \overrightarrow{X_B(t)}), & r < p \\ \overrightarrow{vc} \cdot \overrightarrow{X(t)}, & r \geq p \end{cases} \tag{34}$$

where, UB and LB are the upper and lower boundary searching range, $rand$ and r are random values within [0, 1] range.

Fig. 8 presents the parameter optimization flowchart using SMA optimizer. The algorithm is initiated and the boundary values are set as in (26) and (27). In addition, the objective function of SMA optimizer is set using (24) and (25) for single and two area, respectively. The SMA optimizer starts calculations until reaching maximum iteration value. For each of the iterations, the ISE objective is calculated for slime moulds and their best fitness X_b is accordingly updated. Then, the calculation of W value is made using (34). For each search portion, p, v_b, v_c are updated, and also the corresponding positions are updated. Finally, the obtained optimized controller's parameters are outputted from the SMA optimizer when maximum iterations are reached, and evaluation and comparisons of performance metrics are made in accordance.

V. RESULTS AND DISCUSSIONS

To validate the effectiveness of the proposed coordination and design method, the simulation results have been implemented on different cases including single and two-areas MG systems as shown in Fig. 4 and Fig. 5. The proposed method is based on using hybrid FO controller coordinated with the frequency protection scheme and using optimized controllers' parameters based on SMA optimizer in the presence of the SMES as a VIC device which has a rate limiter of ± 0.3 p.u. without RESs and ± 0.6 with RESs. These studied systems are built using MATLAB-Simulink tool, which is interfaced with the m-file code of the SMA to optimize the control parameters for MG system to achieve the desired objective function. The SMA optimization technique is carried out a laptop computer with processor Intel Core i7 CPU of 2.7 GHz, 64-bit version. It is executed under 100 iteration with size of 30 populations and its performance is compared with other optimization algorithms in literature at 10% step load perturbation (SLP) for single-area and multi-area as depicted in Fig. 9a and Fig. 9b, respectively. It is seen in these figures that SMA technique has achieved the minimum ISE error after around 35 iterations compared to GWO, GA, and PSO algorithms in both single area and multi-area MGs.

Furthermore, the proposed FOTID controller is compared with other conventional and advanced controllers, such as, IO-based I, PI, PID, and FO-based TID, and FOPID controllers through the same coordination during the same conditions of random variations of load and RESs to provide fair validation of its robustness. To preserve the microgrid dynamic security with the proposed control/protection scheme, each area in both single-area and two-area power system case studies has a decentralized FO controller LFC and a SMES PI controller in addition to the implementation of the DFR. The results are investigated for single and two area MG systems under different perturbations over the following cases. Tha obtained optimum controllers' parameters using the SMA optimizer are shown in Table. 2 for single area MG system. The assumed various operating states of step and multi-load variant are implemented in Table. 3, wherein SLP denotes to step load perturbation (SLP).

A. RESULTS OF SINGLE-AREA MG

1) 10% SLP IN SINGLE MG

This scenario aims to validate the effectiveness of the proposed coordination of FOTID controller and DFR system based on the SMA optimizer over the other conventional and advanced control techniques, which are discussed in the literature for comparison. In this case, the studied single-area MG system is examined with a change of 10% demand load at t = 0 s without installing RESs in the system to guarantee a fair comparison with the other I, PI, PID, TID, and FOPID controllers. Fig. 10a visualizes the studied single-area MG system frequency response, where the system frequency fluctuates within the maximum and minimum boundaries of ±1 Hz for the DFR with all the suggested controllers. However, the frequency deviates to a high value at 49.51 Hz with PI controller, while it is 49.66 and 49.68 Hz with PID and I controllers, respectively. Whereas, the value of the

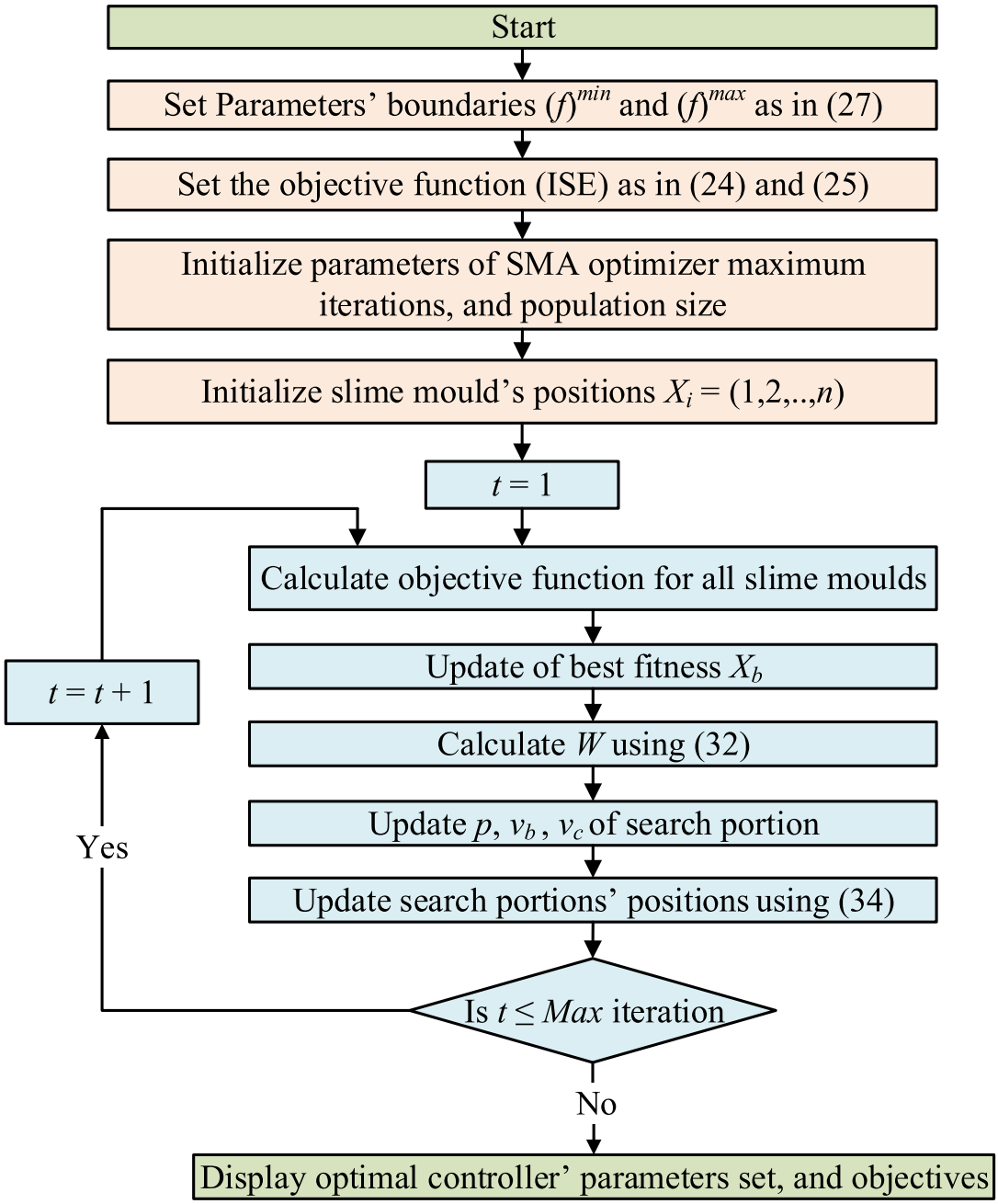

FIGURE 8. Steps of parameters optimization process using SMA optimizer.

TABLE 2. Optimized controllers' parameters in single-area MG.

Controller	Coefficients						
	K_t	K_p	K_i	K_d	λ	μ	n
I	—	—	0.055	—	—	—	—
PI	—	1.526	0.383	—	—	—	—
PID	—	1.785	1.128	1.997	—	—	—
TID	0.288	—	1.124	0.456	—	—	2.79
FOPID	—	1.113	0.599	1.756	0.656	0.788	—
FOTID	0.455	—	0.822	1.231	0.891	0.782	3.56
SMES-PI	—	1.658	1.397	—	—	—	—

frequency deviation of the studied single-area MG system with TID controller has been retained to 49.89 Hz. However, the proposed FO controller provides better performance than the studied classical I, PI, PID, and TID controllers.

TABLE 3. Studied scenarios in single-area MG.

Scenario	Disturbance source	Starting time (sec.)	End time (sec.)	Size (p.u)
(1)	SLP in	0	—	0.1
(2)	SLP out	20	60	0.1
(3)	SLP out	10	—	0.2
(4)	SLP out1	10	—	0.2
	SLP out2	50	—	0.2
(5) case 1	SLP out	0	—	0.05
	wind power	50	—	0.15
(5) case 2	PV power	20	—	0.15
	wind power	70	—	0.22
(5) case 3	SLP out	0 s	—	0.1
	PV power	50	—	0.15
	wind power	80	—	0.25

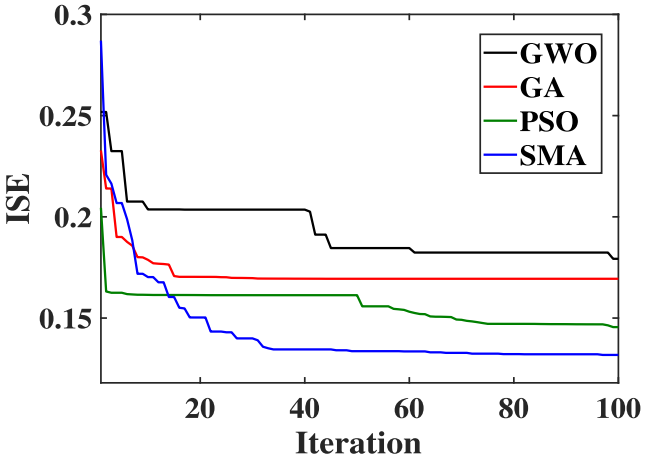

(a) ISE for single area at 10% SLP.

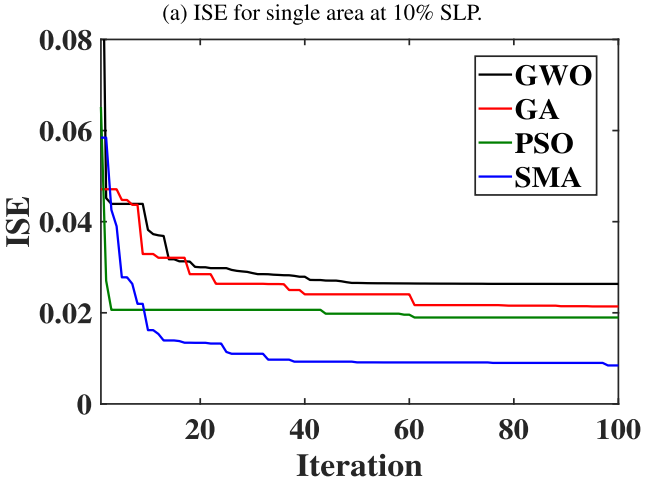

(b) ISE for multi area at 10% SLP.

FIGURE 9. Convergence curves comparisons.

The FOPID controller succeeds to maintain the MG system frequency at 49.96 Hz, while the proposed hybrid FOTID has the best performance in lowering the maximum undershoot to only 49.99 Hz in this case of SLP. The proposed controller is the fastest controller in repressing the frequency fluctuations as it can restore it to its nominal value during 4 s compared with other techniques as noted in Table. 4. Hence, the proposed coordination of FOTID LFC with the fast charging/discharging of SMES effectively succeeds in damping the oscillations of the system frequency and preserving the MG dynamic security without affecting the operation of the DFR system. It can be seen from Fig. 10b and Fig. 10c, that the case of FOTID controller can significantly reduce the area control error which in turn enable the SMES to discharge more power and greatly enhances system frequency and leads to small system transients in comparison with the other control systems.

2) MULTI-STEP LOAD

In this scenario, the single area MG is tested at two step change in load demand, where 10% of load is suddenly shed from the MG system at t = 20 s and restored again after 40 s under the default system parameters. Fig. 11a shows the frequency response of the studied single MG system. It can be noted from this figure that the proposed FOTID controller coordinated with the share of SMES has the best performance response for the MG system as the frequency fluctuations are maintained within ±0.008 Hz. However, the other FOPID controller has ±0.05 Hz deviations in the system frequency. While the TID comes in the third order after the fractional controllers as it can damp the frequency oscillations to ±0.11 Hz, then the PID controller gives a frequency change at ±0.32 Hz. Whereas, the I and PI controllers have the worst performance in this case as the I controller takes long time to restore the frequency to 50 Hz and PI has the highest overshoot and undershoot of ±0.49 Hz. Despite this case includes a sudden two-step load change, the proposed coordination of optimized FOTID LFC based on the SMA optimizer are still preserving the MG system frequency within the range of the control center without the intervention of protection role. This performance of the proposed controller allows the SMES device to cover nearly the whole power shortage compare to other methods, which cover the shortage of electrical power with slow performance as depicted in Fig. 11b and Fig. 11c.

3) LOAD OUTAGE

In order to compare the proposed FOTID LFC with the DFR and with participation of SMES charge/discharge process in a severe case, the efficiency of the single MG system is tested against a sudden change in demand load. Whereas, this scenario considers that around 20% of load is out

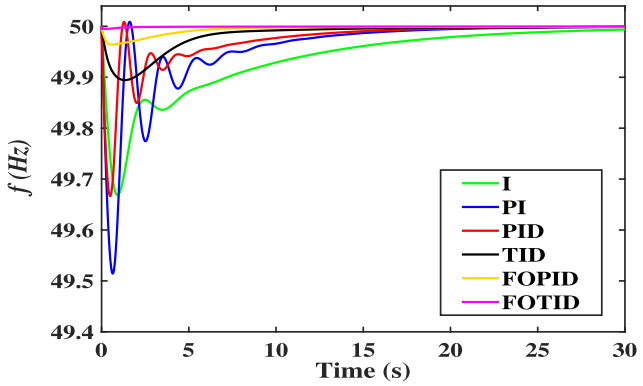

(a) Response of MG frequency

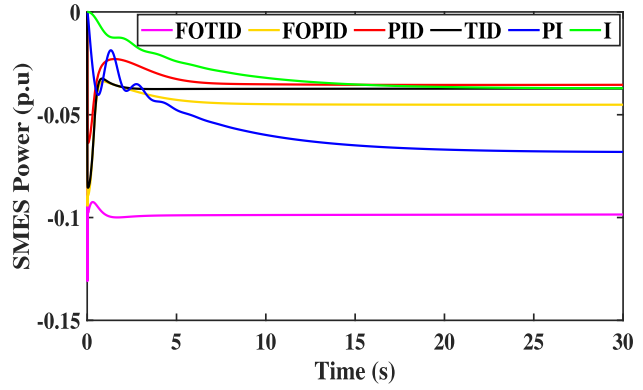

(b) SMES power

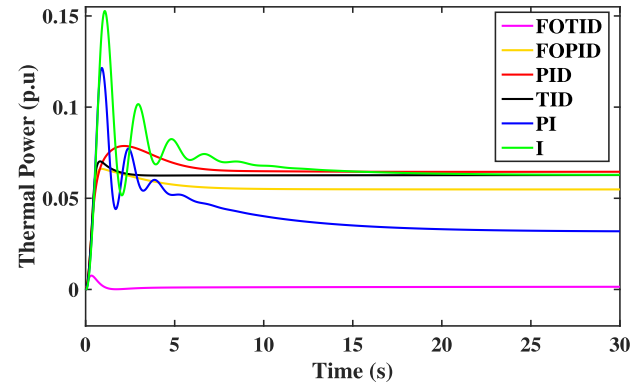

(c) Thermal power

FIGURE 10. Results at 10% SLP.

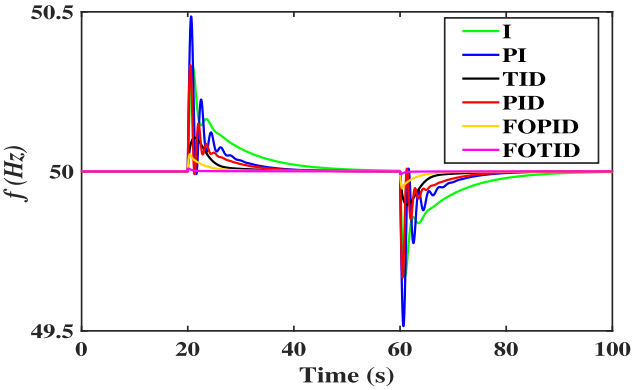

(a) Response of MG frequency

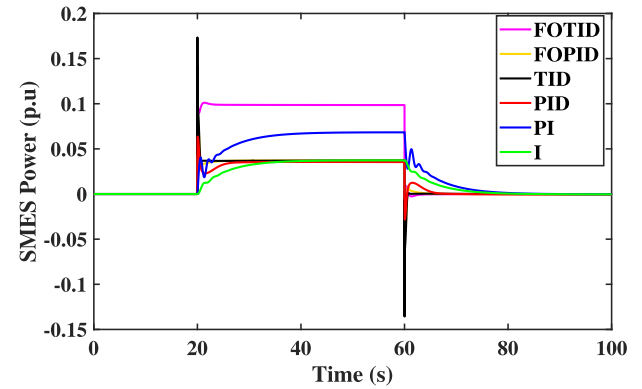

(b) SMES power

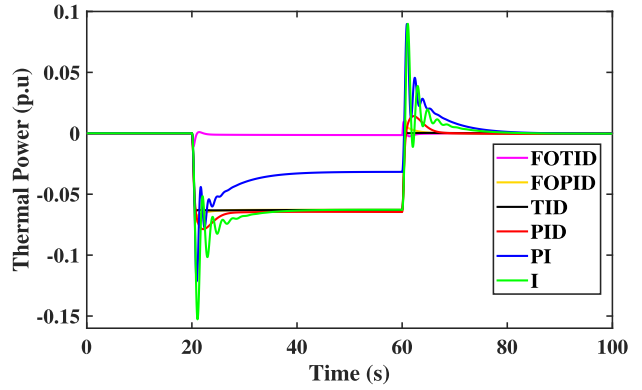

(c) Thermal power

FIGURE 11. Results at multi-step load.

at t = 10 s. The obtained frequency deviations of the proposed single MG system for this case are depicted in Fig. 12 with different control strategies, such as I, PI, PID, TID, and FOPID controllers based on the SMA optimizer. From this figure, it is obvious that the MG frequency response for both I and PI controllers is not maintained within the control limits and exceed 51 Hz. Therefore, the DFR protection system is activated in this case and sent a tripping signal as depicted in Fig. 12. While using the PID and TID controllers can face this severe load change and keep the system frequency within the allowable limits of control and protection centers with overshoots of 0.75 Hz and 0.48 Hz, respectively. Moreover, the TID is faster than PID as it needs for 12 s to restore the frequency to its nominal value, while the PID controller needs more than 34 s. On the other side, the FO controllers have robust performance, where the system frequency is limited to 0.16 Hz using the FOPID controller and 0.04 Hz with FOTID controller. Hence, the proposed hybrid FO with the SMES share in the LFC loop has the minimum frequency overshoot and the less settling time compared to all the other studied controllers.

4) SEVERE LOAD OUTAGE CASE

The capability of the suggested coordination based-LFC and SMES using the SMA optimizer beside the action from the DFR frequency protection system is evaluated and tested

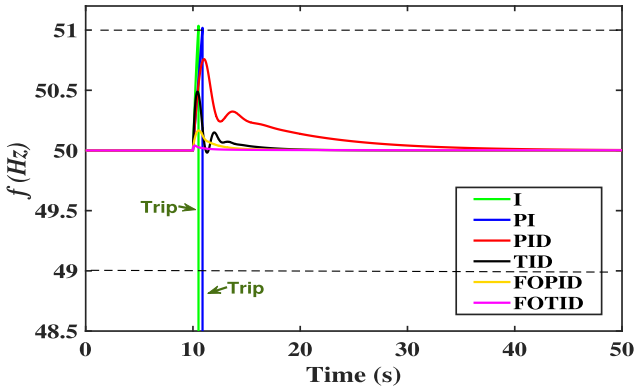

FIGURE 12. Response of MG frequency at load outage.

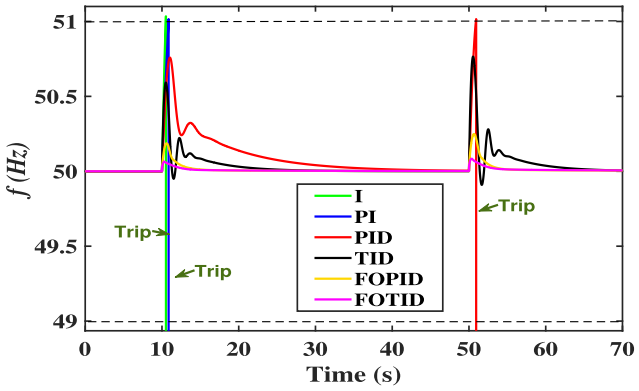

FIGURE 13. Response of MG frequency at severe load outage case.

under the impact of an extreme case of load outage. In which, the studied single MG system is examined under the outage of 20% of demand load at 10 s and other of 20% outage at 50 s. Fig. 13 shows the frequency performance of this severe disturbance case. The I and PI controllers, as LFC beside the virtual inertia share from SMES, cannot damp the system frequency under 51 Hz as seen from this figure. Therefore, an interfered action occurs from the DFR side for tripping signal at the first instant of load outage at t = 10 s. Moreover, the PID controller cannot withstand the second load outage at t = 50 s and it does not maintain the MG frequency beyond the control limits under ±1 Hz and further tripping action from the DFR is occured.

However, the coordination of TID controller in LFC loop with SMES support can keep the frequency fluctuations at 50.59 Hz and 50.77 Hz at times of 10 s. and 50 s with long settling time, respectively. On the other hand, the FOPID controller succeeded to damp the frequency deviations to 50.19 Hz at 10 s and to 50.25 Hz at 50 s without using the tripping action from the DFR. Furthermore, the proposed FOTID controller can restore the MG frequency to 50.06 Hz and 50.08 Hz at 10 s and 50 s, respectively. This means that the impact of the proposed FOTID for LFC in addition to the fast charge/discharge process of SMES is fastest in damping down the MG frequency deviations within an acceptable limit for the control ad protection centers.

5) IMPACT OF RESs

The main objective of this scenario is to demonstrate the performance of the studied single-area MG system at high emergency cases under the impact of RESs variations, which acts as the main component of the actual MG. Including RESs leads to low power system inertia due to existing inverter-based structures in a power microgrid systems and the absence of rotational masses as well, which in turn introduces several stability, reliability, and coordination problems for MG operation. Therefore, the studied single MG area is examined by installing high fluctuated PV and wind generation units as shown in Fig. 14 and their operating conditions during different cases are listed in Table. 3. This scenario includes three different sub-scenarios for RESs beside demand load changes as following:

- **Case 1:** In addition to the load disturbance at initial time of simulation with 5% SLP outage, the wind generation unit is connected at t = 50 s. In this case, the performance of all studied controllers is evaluated in Fig. 15a. Whereas, the I controller can suppress the high frequency overshoot deviations at initial time of simulation but cannot restore it to an acceptable value at instant of wind insertion (t = 50 s). Hence, the proposed frequency relay protects the MG system with this controller by sending a trip signal for disconnection as depicted in Fig. 15a. While, the PI controller succeeded to maintain the frequency deviations within the allowable range of control action without need for DRF interfacing. Furthermore, the PID and TID controllers gave nearly similar performance in this case by damping the frequency deviation to 50.05 Hz at t = 0 s, and to 50.19 Hz and 50.17 Hz at t = 50 s, respectively. However, the most efficient and the fastest in restoring the system frequency near its nominal value is being the FO controllers, where the FOPID can suppress the frequency fluctuations to 50.025 Hz and 50.11 Hz at 0 s and 50 s, respectively. Moreover, using FOTID makes the system with the proposed coordination scheme offers more effectiveness and well performance with the lowest oscillation and minimum settling time.
- **Case 2:** To perform more severe scenario for testing the effectiveness of the proposed LFC coordination with SMES and monitoring system frequency via the DFR device, the studied single MG area is subjected to multiple RESs. Therefore, both wind and PV power plants are employed in the MG system in this case, where the PV generation is connected to the system at t = 20 s and the connection of wind unit is at t = 70 s. Fig. 15b shows the frequency response of the studied MG power system for this case. It is obvious that the I controller tried to retain the frequency beyond the control center limits. However, after nearly 7 s, the I controller failed and the frequency exceeded the control limits despite the SMES high sharing power in this case as depcited in Fig. 16 and the frequency value entered the range of

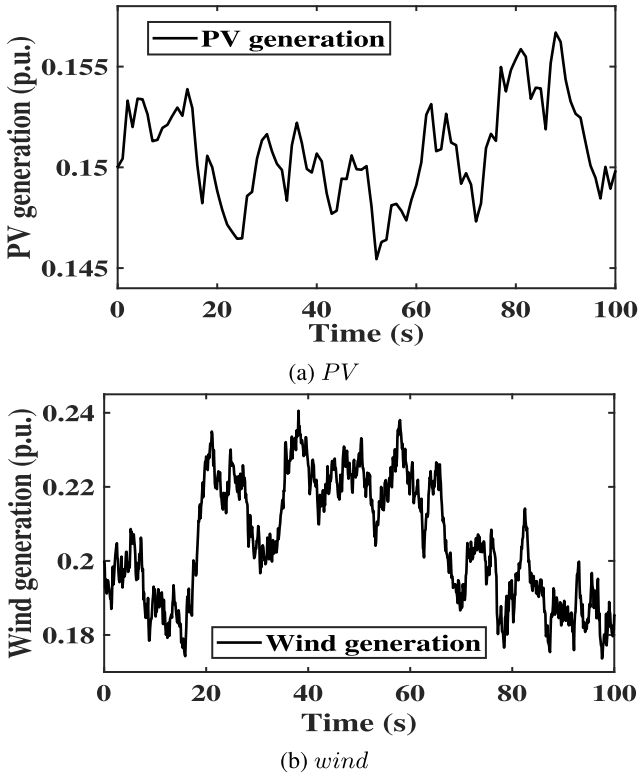

FIGURE 14. Power generation of RES.

the DFR protective relaying, which is being energized and sent a trip signal to the breaker in this situation. Furthermore, the PI controller can damp the frequency deviations at the PV connection instant (t = 20 s), however it cannot withstand the high penetration levels of RESs by inserting wind generation unit at t = 70 s, and also the system frequency changes to be more than 51 Hz, which is the reason for a tripping signal from the DFR as shown in Fig. 15b at 70 s. While the PID controller succeeded to keep the frequency fluctuations within the allowable limits of control action. However, it suffers from protracted damped vacillations especially at the instant of wind generation connection at 70 s. However, the TID and FOPID controllers give better performance than the PID, PI, and I by decreasing the system frequency aberration of the studied single-area MG system to 50.22 Hz and 50.11 Hz at 20 s and 50.32 Hz and 50.18 Hz, respectively. Otherwise, the proposed FOTID exhibits the best performance in lowering the frequency overshoot to 50.045 Hz and 50.06 Hz at PV and wind connections instants, respectively as it allowed the SMES device in the LFC loop to store the excessive power form PV and wind instantaneously compared to other some controllers which supported the LFC but with delay in charging as shown in Fig. 16b. Therefore, it has the most robust performance compared to other controllers in terms of overshoot, undershoot, settling time as summarized in Table. 5.

- **Case 3:** To make a drastic scenario for the capability of the single MG system, it is tested under the impact of high penetration level of RESs. Therefore, this case includes a step load out at initial instant beside PV generation connection at t = 50s and increasing the penetration of wind generation at t = 80s. Fig. 15c shows the obtained performance comparisons of the proposed and suggested controllers. The proposed coordination of FOTID LFC with SMES based on the new modified MPA possesses the minimum overshoot/undershoot in the MG frequency deviations and maintain the frequency value within the permissible limits of control and protection along the simulation time without any necessity for the DFR action. While the worst performance is achieved by the I controller as the frequency reached to 51 Hz from the first share of RESs at t = 50s when the PV generation is connected and hence a tripping action from the DFR is occurred. Furthermore, the PI and PID controllers cannot withstand the high penetration level of wind generation at t = 80s as the Mg system frequency deviates and exceeds the allowable limits of control and enters the DFR range over 1 Hz. Therefore, the frequency protective relay sent a trip indicative to the generator circuit breaker at this instant of connecting high fluctuated wind generation. While, the TID and FOPID succeeded to keep the frequency deviations within the acceptable range of control and protection systems during the three disturbance steps in this scenario. However, they came in the second and third orders after the proposed FOTID, which has a remarkable decrease in the settling time measurement and has the minimum undershoot and overshoot related to the other comparable controllers.

B. RESULTS OF MULTI-AREA MG SYSTEM

In this subsection, the suggested coordination of the hybrid FO controller with the SMES charge/discharge process in the presence of monitoring DFR protective device has been applied to the interconnected MG system as shown in the dynamic model in Fig. 5. Moreover, the proposed LFC coordination is compared with the same conventional and advanced control techniques as in the previous sections such as, I, PI, PID, TID, FOPID controllers. All control parameters are tuned based on the SMA optimizer as summarized in Table. 6. To investigate the suggested control/protection coordination on the multi-area MG system, five different scenarios are applied as in the following subsections.

1) 10% SLP IN MULTI-MGs (SCENARIO 1)

The effectiveness of the proposed coordination of LFC using the FOTID controller, energy storage device, and DFR system is evaluated in a multi-area MG system by applying 10% SLP in this scenario at area *a*. The variation of system frequency is depicted in Fig. 17. It can be noted from this figure that the frequencies in area *a* and *b* are significantly deviating at high values of 49.63 Hz and 49.7 Hz, respectively in case

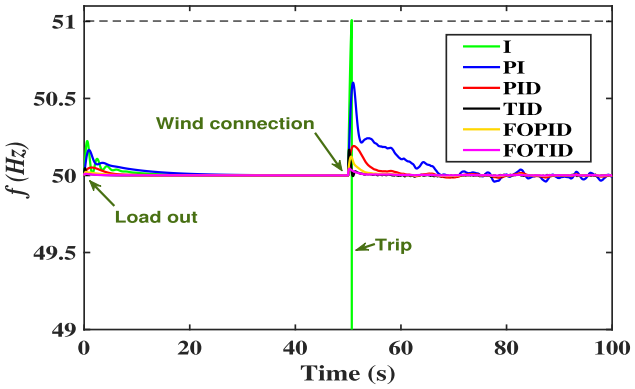

(a) f_{Case1}

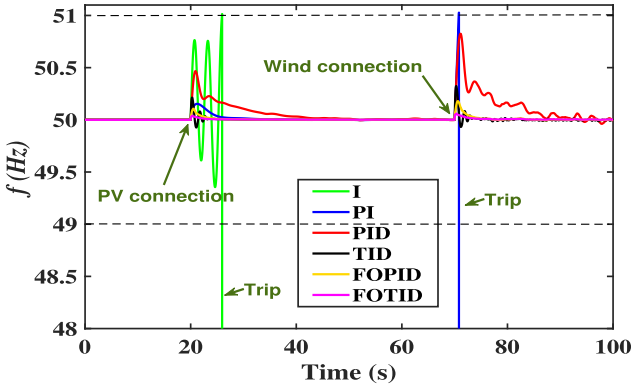

(b) f_{Case2}

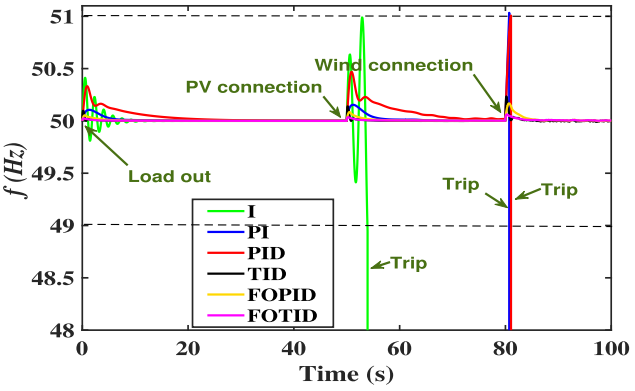

(c) f_{Case3}

FIGURE 15. Response of MG frequency for RES scenarios.

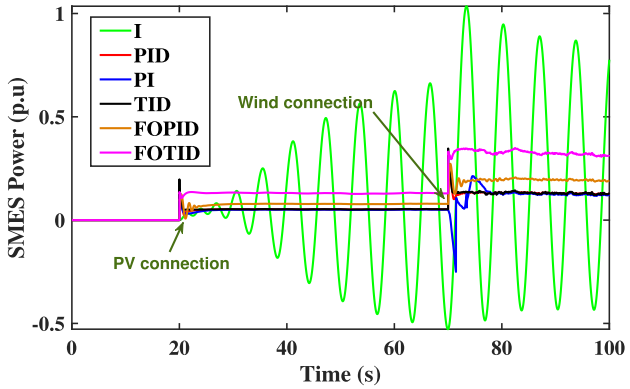

(a) SMES power

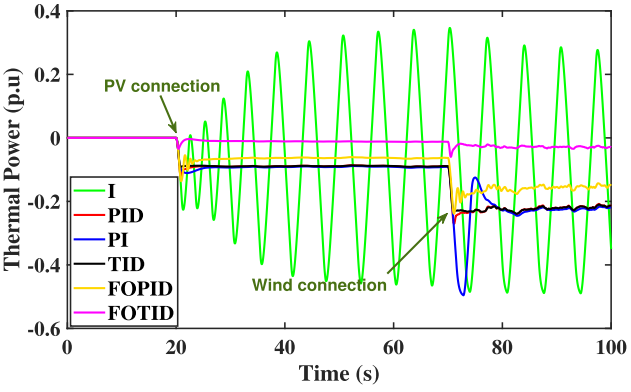

(b) Thermal power

FIGURE 16. Output power at f_{Case2}.

TABLE 4. Performance measurements for the Load disturbance scenarios in single-area.

Scenario	Controller	f		
		MO	MU	ST (sec.)
(1) (at 0 sec.)	I	—	49.68	>35
	PI	50.01	49.51	35
	PID	50.01	49.66	27
	TID	—	49.89	20
	FOPID	—	49.96	13
	FOTID	—	49.99	4
(2) (at 20 sec.)	I	50.33	50.16	>40
	PI	50.49	50.23	28
	PID	50.33	50.15	24
	TID	50.11	—	23
	FOPID	50.05	—	15
	FOTID	50.008	—	6
(3) (at 10 sec.)	I	51.04	—	trip
	PI	51.02	—	trip
	PID	50.76	50.32	35
	TID	50.48	50.15	15
	FOPID	50.17	—	11
	FOTID	50.04	—	7
(4) (at 10 sec.)	I	51.04	—	trip
	PI	51.02	—	trip
	PID	50.76	50.32	trip at 50 s
	TID	50.59	50.22	18
	FOPID	50.19	—	10
	FOTID	50.06	—	7

of using I controller. Furthermore, the PI controller gives frequency deviations at 49.65 Hz for area *a* and 49.76 Hz for area *b*. While the PID has a value of 49.69 Hz in area *a* and 49.72 Hz in area *b*. However, it is better than I and PI controllers in settling time to nominal frequency value. TID controller shows a better performance than the previous controllers as it has less undershot values of 49.8 Hz in area *a* and 49.93 Hz in area *b*. On the other hand, the FO controllers have the best performance in this case compared to other controllers as the FOPID can damp the frequency deviations to 49.89 Hz and 49.95 Hz for area *a* and area *b*, respectively. However, the FOTID controller is the best one as it has the minimum undershoot values 49.97 Hz in area *a* and 49.99 Hz in area *b* and the less settling time as noted in Table 8. It can be concluded in this case that the frequency deviations in both areas do not exceed the set protection value. Therefore,

TABLE 5. Performance measurements of the RESs impact scenarios in single-area.

Scenario (5)	Controller	f		
		MO	MU	ST (sec.)
case (1) (at 50 sec.)	I	51.01	—	trip
	PI	50.61	50.24	OS
	PID	50.19	50.03	OS
	TID	50.16	50.02	22
	FOPID	50.12	—	12
	FOTID	50.05	—	9
case (2) (at 20 sec.)	I	51.01	—	trip
	PI	50.17	—	trip at 70 s
	PID	50.47	50.23	35
	TID	50.22	50.08	14
	FOPID	50.11	—	12
	FOTID	50.04	—	7
case (3) (at 80 sec.)	I	—	—	trip at 50 s
	PI	51.03	—	trip
	PID	51.01	—	trip
	TID	50.24	50.04	9
	FOPID	50.17	—	11
	FOTID	50.06	—	8

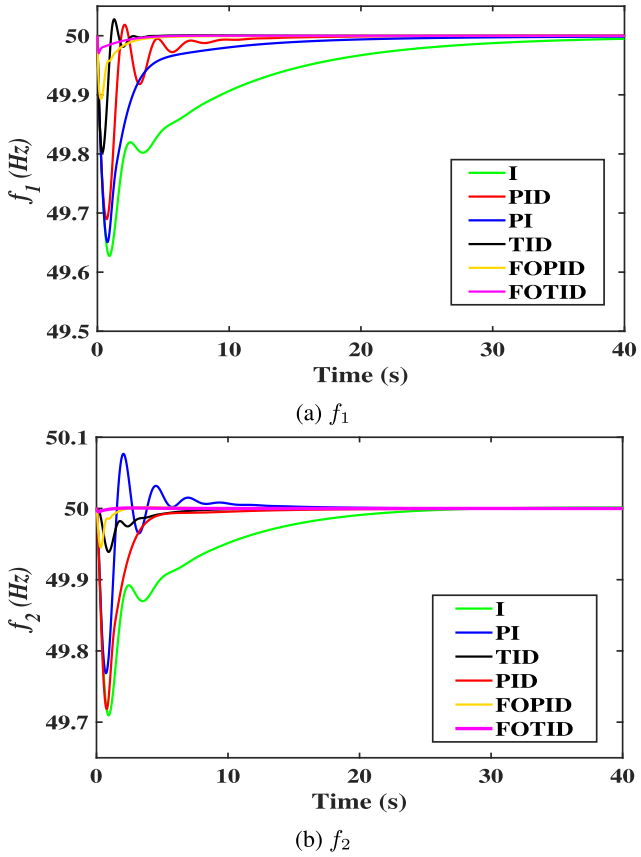

FIGURE 17. Response of Multi-MGs frequency at 10% SLP case.

the LFC coordination succeeded to readjust the frequency to 50 Hz without the need for protection action from the DFR.

2) LOAD OUTAGE IN MULTI-MGs (SCENARIO 2)

In this case, the islanded multi-area MG system behavior is tested by applying the same load change as the previous scenario except that the all 40% load demand change is at area *a* only at time 10 s. Thence, there are two tripping cases

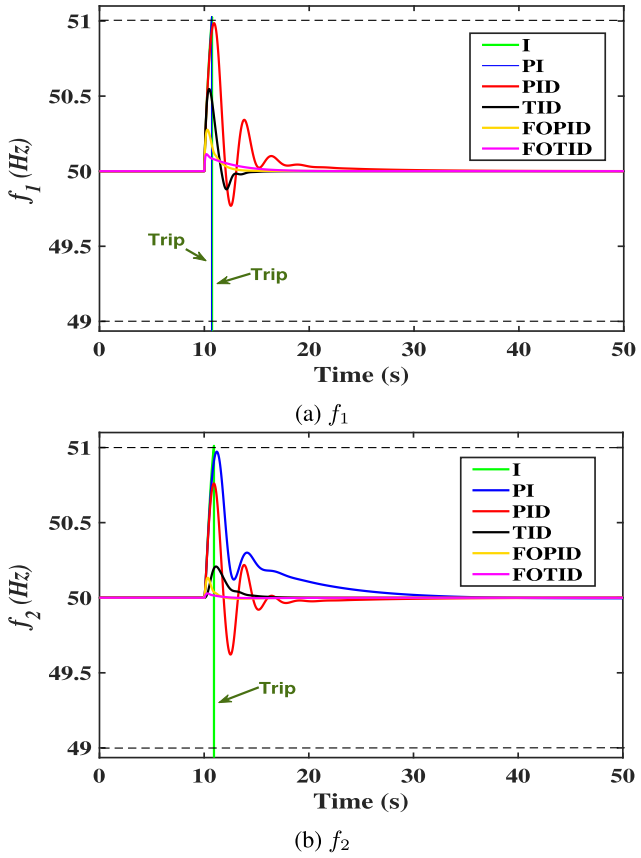

FIGURE 18. Response of Multi-MGs frequency at severe load outage case.

from the DFR in this extreme case when using the I and PI controllers. It can be seen from Fig. 18 the effect of this huge load change on the performance of these controllers. The PI controller does not have a trip action in case of area *b* due to the change of load in area *a*. Furthermore, the PID controller gave worse performance as the frequency error is 0.99 Hz in area *a* and 0.77 Hz in area *b* with long settling time. In contrast, by employing the TID and fractional FOPID controllers based-SMA coordinated with the SMES contribution; the amplitude of the system fluctuations is within the permissible limits of MG system frequency. As well, utilizing FOTID controller maintains the frequency deviation around 0.1 Hz in area *a* and 0.03 Hz in area *b* with faster performance than the above-mentioned controllers. It can be concluded from these results that the coordination of hybrid FOTID LFC and SMES based on SMA optimizer with considering the DFR represents the best combination compared to same coordination of other controllers in the LFC loop.

3) RESs IMPACTS IN MULTI-MGs (SCENARIO 3)

This scenario is implemented to reveal the performance of the two-area MG system when utilizing the suggested coordination of optimized LFC and SMES based on the SMA optimizer and further the effect of DFR in protecting the power system during high emergency cases. Therefore, this scenario is divided into different sub-scenarios of different

TABLE 6. Optimized parameters in Multi-area MG.

Controller	Area	Coefficients						
		K_t	K_p	K_i	K_d	λ	μ	n
I	Area a	—	—	0.058	—	—	—	—
	Area b	—	—	0.123	—	—	—	—
PI	Area a	—	0.851	0.657	—	—	—	—
	Area b	—	0.811	0.594	—	—	—	—
PID	Area a	—	2.678	0.569	1.745	—	—	—
	Area b	—	1.957	0.855	1.225	—	—	—
TID	Area a	0.188	—	0.124	0.409	—	—	3.08
	Area b	0.224	—	0.713	0.587	—	—	2.77
FOPID	Area a	—	1.212	0.547	1.564	0.593	0.842	—
	Area b	—	1.001	0.492	1.211	0.472	0.512	—
FOTID	Area a	0.525	—	1.1	1.524	0.854	0.921	3.21
	Area b	0.124	—	0.925	0.745	0.752	0.624	2.91
SMES-PI	Area a	—	2.548	1.754	—	—	—	—
	Area b	—	1.954	1.878	—	—	—	—

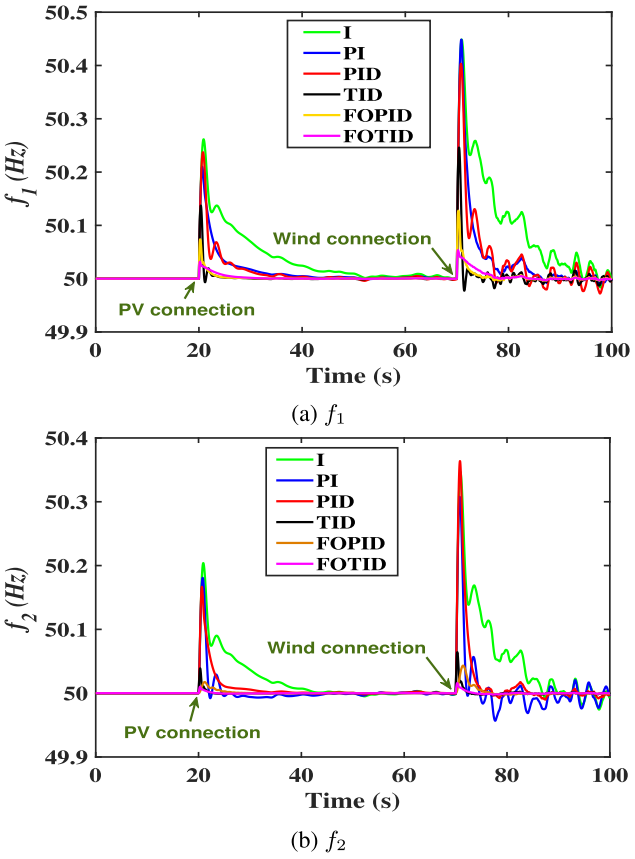

(a) f_1

(b) f_2

FIGURE 19. Response of Multi-MGs frequency for RES case 1.

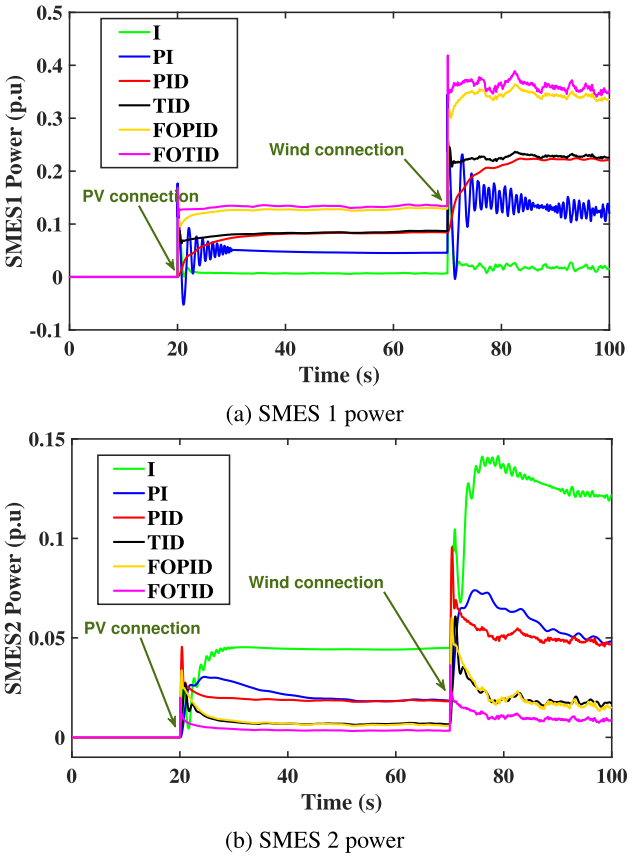

(a) SMES 1 power

(b) SMES 2 power

FIGURE 20. Output power at RES case 1.

penetration levels from the PV and wind generation units to validate the effectiveness of the proposed technique. The operation conditions of PV and wind penetration during different cases are listed in Table. 7.

- **Case 1:** The PV power generation shared with the wind generation in this case with p.u. percentage as noted in Table. 7. Whereas the PV is connected at t = 20 s and wind is connected at t = 70 s. It is obvious from Fig. 19 that the frequencies of the MG system in both areas have more deviations and slower settling time in case of I, PI, and PID controllers with slightly high overshoots compared to other controllers. However, the TID controller provides satisfactory results with reasonable capability in damping out the frequency oscillations in area a and area b. On the other hand, the FOPID and FOTID controllers succeed at treating this contingency regardless of the double share from PV and wind power generation units. Furthermore, the proposed FOTID based-SMA with the aid of fast charge/discharge of SMES device, which can handle the increase of electrical power coming from PV and wind generation in this case as seen in Fig. 20a and Fig. 20b. Therefore,

TABLE 7. Multiple operating conditions of Multi-area MG.

Scenario	Disturbance source	Area	Starting time (sec.)	End time (sec.)	Size (p.u)
(1)	SLP in	Area a	0	—	0.2
(2)	SLP out	Area a	10	—	0.4
(3) case 1	PV power	Area a	20	—	0.15
	wind power	Area a	70	—	0.25
(3) case 2	PV power	Area a	20	—	0.2
	PV power	Area b	20	—	0.2
	wind power	Area a	70	—	0.25
	wind power	Area b	70	—	0.25
(3) case 3	SLP out	Area a	40	—	0.15
	wind power	Area a	70	—	0.25
	PV power	Area a	40	—	0.2
	SLP in	Area b	0 s	60	0.2
	wind power	Area b	70 s	—	0.25

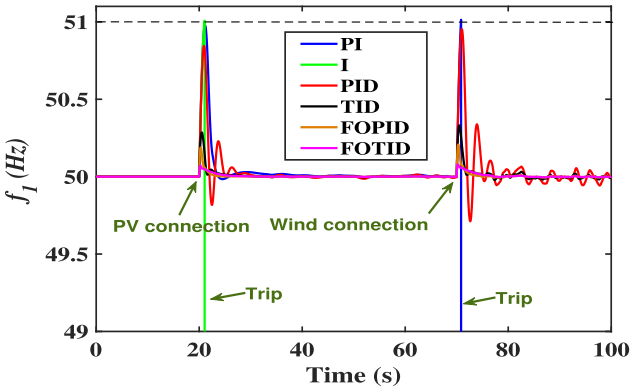

(a) f_1

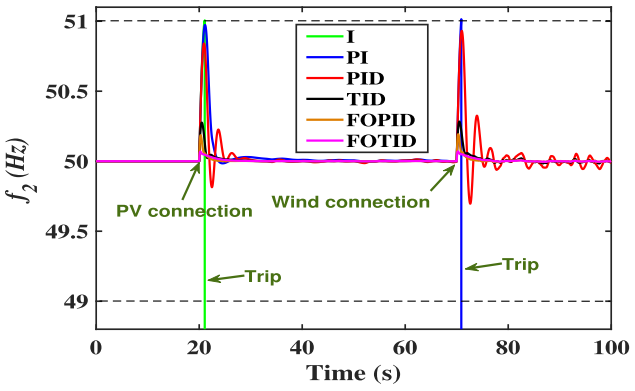

(b) f_2

FIGURE 21. Response of Multi-MGs frequency for RES case 2.

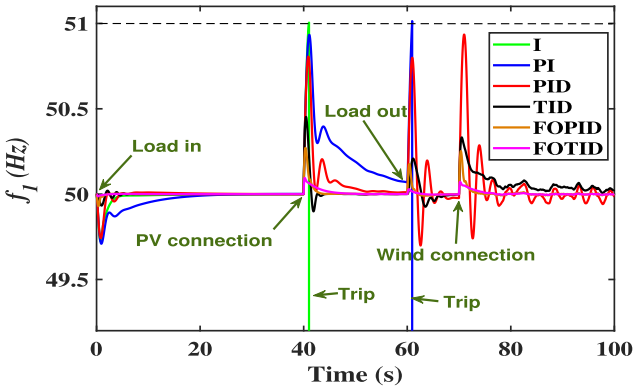

(a) f_1

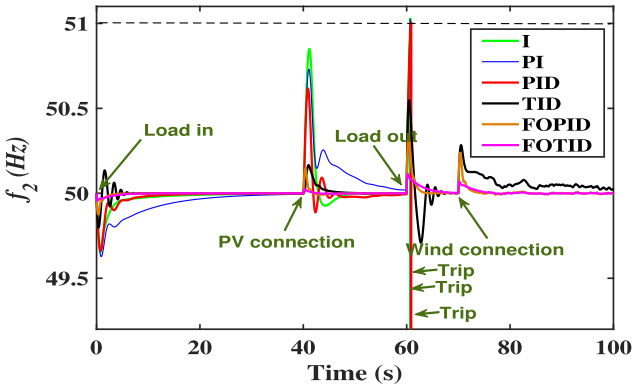

(b) f_2

FIGURE 22. Response of Multi-MGs frequency for RES case 3.

it can improves the whole dynamic system stability by damping the frequency deviations to only 0.03 Hz and 0.05 Hz at PV and wind connections, respectively in both areas.

- **Case 2:** This case has the same steps of the previous scenario with increasing the penetration level of RESs as listed in Table. 7. It can be noted from the obtained result in Fig. 21 that there is an early trip action from the DFR device at t = 20 s during the connection of high share from PV generation in both areas while using the I controller in addition to another trip signal at t = 70 s during the connection of wind power generation in case of using the PI controller. Moreover, the PID controller has lower performance in damping the high frequency fluctuations with suffering from long settling time value for frequency oscillations. While the TID and the FOPID controllers provide suitable performance and faster settling time than the I, PI, and PID controllers with reasonable aptitude at damping out the MG frequency vacillations. The proposed hybrid FOTID controller exhibits better dynamic performance to damp out the frequency and power oscillations in comparison to other previous controllers. The proposed coordination between the FOTID-LFC controller and SMES based on the SMA optimizer represents the best combination compared to the other schemes.

TABLE 8. Performance measurements for the Load disturbance scenarios in Multi-area MG.

Scenario	Controller	f_a			f_b		
		MO	MU	ST (sec.)	MO	MU	ST (sec.)
Scenario (1) (at 0 sec.)	I	49.82	49.63	>40	49.89	49.71	29
	PI	—	49.65	>35	50.08	49.77	24
	PID	50.02	49.69	21	—	49.72	21
	TID	50.03	49.81	13	49.98	49.94	16
	FOPID	—	49.89	10	—	49.95	7
	FOTID	—	49.97	8	—	49.99	5
Scenario (2) (at 10 sec.)	I	51.02	—	trip	51.01	—	trip
	PI	51.03	—	trip	50.97	50.31	36
	PID	50.98	49.77	34	50.76	49.62	26
	TID	50.55	49.88	19	50.21	—	11
	FOPID	50.28	—	16	50.13	—	8
	FOTID	50.11	—	11	50.03	—	5
Scenario (3) case (1) (at 70 sec.)	I	50.45	50.12	OS	50.35	50.02	OS
	PI	50.45	50.04	OS	50.31	49.96	OS
	PID	50.40	50.05	OS	50.36	50.02	OS
	TID	50.25	49.98	OS	50.07	50.01	14
	FOPID	50.13	—	16	50.04	50.01	15
	FOTID	50.05	—	14	50.02	—	10
Scenario (3) case (2) (at 20 sec.)	I	51.01	—	trip	51.01	—	trip
	PI	50.98	49.98	trip at 70 sec.	50.97	49.98	trip at 70 sec.
	PID	50.85	49.82	37	50.84	49.82	27
	TID	50.28	50.05	13	50.27	50.05	12
	FOPID	50.19	—	9	50.19	—	10
	FOTID	50.07	—	10	50.07	—	10
Scenario (3) case (3) (at 60 sec.)	I	—	—	trip at 40 sec.	51.02	—	trip
	PI	51.01	—	trip	51.02	—	trip
	PID	50.80	49.70	OS	51.01	—	trip
	TID	50.21	49.93	OS	50.55	49.71	OS
	FOPID	50.18	50.03	8	50.33	—	5
	FOTID	50.09	—	7	50.11	—	9

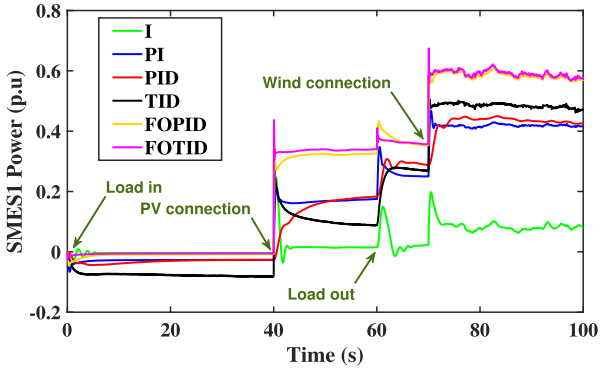

(a) SMES 1 power

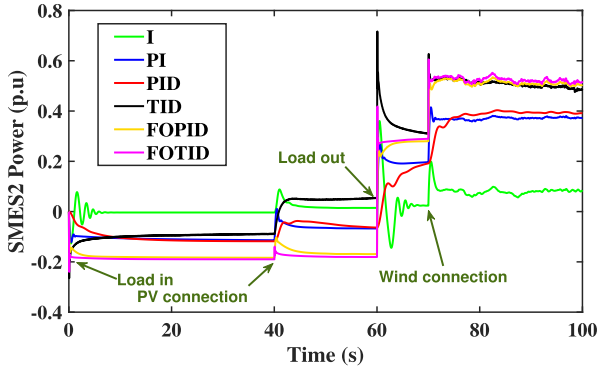

(b) SMES 2 power

FIGURE 23. Output power at RES case 3.

- **Case 3:** This scenario considers further validation of the new proposed coordination strategy of FOTID controller performance and its cooperation with SMES sharing level. Therefore, the multi-area MG system is evaluated and revealed under the impact of drastic multi-SLP at t = 0 s and t = 60 s. In addition, the impact of RESs with their variability and intermittency in the generation are addressed in this case. Where the PV generation unit with high penetration level as listed in Table 7 is connected at t = 40 s and connection of wind power generation at t = 70 s. Fig. 22 shows more frequency fluctuating and larger transient deviation of the studied MG system during low system inertia condition due to high penetration level of PV and wind generation units. It can be distinguished from this figure that the I and PI controllers have lower performance as the DFR takes a trip action twice in area *a* at 40 s with I controller and at 60 s with PI controller. Furthermore, there is a trip signal for three controllers in area *b* at instant of load outage at t = 60 s for I, PI, and PID controllers, respectively. Moreover, the TID controller with SMES support tries to maintain the frequency beyond the safety control limits, however it cannot restore the system frequency to its nominal value in this scenario due to slow performance of TID and SMES in the LFC loop as shown in Fig. 23. On the other hand, the FOPID and FOTID controllers have better dynamic response in restoring the frequency deviations in both areas but with smaller deviations for FOPID then FOTID as the SMES coordination can compensate the power in this severe case of load in and out beside the high penetration of RESs. Fig. 23a and Fig. 23b show the difference in SMES process in both

areas with the proposed technique in comparison with different LFC types. Therefore, the proposed coordination in this work proved that it can achieve suitable efficacy in regulating the power system frequency and enhancing the dynamical behavior of multi-area MG electrical power network with high penetration levels of RESs without the intervention of the DFR protection system in all previous scenarios.

VI. CONCLUSION

A novel coordination between LFC based-FOTID controller, energy storage system based-SMES, and frequency protection system based-DFR is proposed in this paper to enhance the transient stability of single and multi-area electrical MG networks. The recently-introduced SMA technique is applied for tuning the parameters of the new proposed coordination such as the FOTID controller and the other comparable controllers. Moreover, the PI controller is tuned simultaneously using the SMA for controlling SMES in each area. To prove the robustness of the proposed coordination, mixed renewable sources such as PV and wind generators with their fluctuations and uncertainties are considered in this work in addition to the existing nonlinearities and uncertainties of demand load variations in single-area and multi-area MG power systems. The obtained results verify that the proposed coordination of FOTID LFC with SMES participation has higher efficiency in maintaining system frequency at its nominal value than the other coordination types such as the conventional I, PI, PID, TID and advanced FOPID controllers. Whereas, the proposed technique succeeded to readjust the MG frequency deviations to its allowable limits under all different transient conditions such as load variations and different RESs penetration levels. Meanwhile, in some cases of large disturbances, the other literature methods cannot maintain the frequency stability within the acceptable range of control and protection system, which in turn causes the DFR to trip the generation units. Therefore, the proposed SMA-based optimized FOTID controller coordinated with SMES and DFR system can achieve better dynamic performance of MG system frequency with high penetration levels of RESs. Future research includes the study of voltage stability with frequency stability under the proposed controller, studying the optimum sizing and allocation of SMES devices, and comparing the performance of SMES with other existing energy storage devices.

REFERENCES

[1] S. Oshnoei, A. Oshnoei, A. Mosallanejad, and F. Haghjoo, "Contribution of GCSC to regulate the frequency in multi-area power systems considering time delays: A new control outline based on fractional order controllers," *Int. J. Electr. Power Energy Syst.*, vol. 123, Dec. 2020, Art. no. 106197.

[2] A. Elmelegi, E. A. Mohamed, M. Aly, E. M. Ahmed, A.-A.-A. Mohamed, and O. Elbaksawi, "Optimized tilt fractional order cooperative controllers for preserving frequency stability in renewable energy-based power systems," *IEEE Access*, vol. 9, pp. 8261–8277, 2021.

[3] M. Adibi and J. Van Der Woude, "Secondary frequency control of microgrids: An online reinforcement learning approach," *IEEE Trans. Autom. Control*, vol. 67, no. 9, pp. 4824–4831, Sep. 2022.

[4] W. Zhong, G. Tzounas, and F. Milano, "Improving the power system dynamic response through a combined voltage-frequency control of distributed energy resources," *IEEE Trans. Power Syst.*, early access, Feb. 4, 2022, doi: 10.1109/TPWRS.2022.3148243.

[5] S. M. Said, M. Aly, B. Hartmann, and E. A. Mohamed, "Coordinated fuzzy logic-based virtual inertia controller and frequency relay scheme for reliable operation of low-inertia power system," *IET Renew. Power Gener.*, vol. 15, no. 6, pp. 1286–1300, Feb. 2021.

[6] L. Jin, Y. He, C.-K. Zhang, X.-C. Shangguan, L. Jiang, and M. Wu, "Robust delay-dependent load frequency control of wind power system based on a novel reconstructed model," *IEEE Trans. Cybern.*, vol. 52, no. 8, pp. 1–12, Feb. 2021.

[7] M. Khudhair, M. Ragab, K. M. AboRas, and N. H. Abbasy, "Robust control of frequency variations for a multi-area power system in smart grid using a newly wild horse optimized combination of PIDD2 and PD controllers," *Sustainability*, vol. 14, no. 13, p. 8223, Jul. 2022.

[8] E. M. Ahmed, A. Elmelegi, A. Shawky, M. Aly, W. Alhosaini, and E. A. Mohamed, "Frequency regulation of electric vehicle-penetrated power system using MPA-tuned new combined fractional order controllers," *IEEE Access*, vol. 9, pp. 107548–107565, 2021.

[9] A. M. Ersdal, L. Imsland, and K. Uhlen, "Model predictive load-frequency control," *IEEE Trans. Power Syst.*, vol. 31, no. 1, pp. 777–785, Jan. 2016.

[10] İ. Kocaarslan and E. Çam, "Fuzzy logic controller in interconnected electrical power systems for load-frequency control," *Int. J. Electr. Power Energy Syst.*, vol. 27, no. 8, pp. 542–549, Oct. 2005.

[11] C. S. Rao, S. S. Nagaraju, and P. S. Raju, "Automatic generation control of TCPS based hydrothermal system under open market scenario: A fuzzy logic approach," *Int. J. Elect. Power Energy Syst.*, vol. 31, no. 7, pp. 315–322, 2009.

[12] S. K. Pandey, S. R. Mohanty, and N. Kishor, "A literature survey on load–frequency control for conventional and distribution generation power systems," *Renew. Sustain. Energy Rev.*, vol. 25, pp. 318–334, Sep. 2013.

[13] R. Shankar, S. R. Pradhan, K. Chatterjee, and R. Mandal, "A comprehensive state of the art literature survey on LFC mechanism for power system," *Renew. Sustain. Energy Rev.*, vol. 76, pp. 1185–1207, Sep. 2017.

[14] P. N. Topno and S. Chanana, "Differential evolution algorithm based tilt integral derivative control for LFC problem of an interconnected hydrothermal power system," *J. Vibrat. Control*, vol. 24, no. 17, pp. 3952–3973, Jul. 2017.

[15] C. K. Shiva, G. Shankar, and V. Mukherjee, "Automatic generation control of power system using a novel quasi-oppositional harmony search algorithm," *Int. J. Electr. Power Energy Syst.*, vol. 73, pp. 787–804, Dec. 2015.

[16] B. Mohanty, S. Panda, and P. K. Hota, "Controller parameters tuning of differential evolution algorithm and its application to load frequency control of multi-source power system," *Int. J. Electr. Power Energy Syst.*, vol. 54, pp. 77–85, Jan. 2014.

[17] E. A. Mohamed, E. M. Ahmed, A. Elmelegi, M. Aly, O. Elbaksawi, and A.-A. A. Mohamed, "An optimized hybrid fractional order controller for frequency regulation in multi-area power systems," *IEEE Access*, vol. 8, pp. 213899–213915, 2020.

[18] K. Singh, M. Amir, F. Ahmad, and M. A. Khan, "An integral tilt derivative control strategy for frequency control in multimicrogrid system," *IEEE Syst. J.*, vol. 15, no. 1, pp. 1–12, May 2020.

[19] A. Delassi, S. Arif, and L. Mokrani, "Load frequency control problem in interconnected power systems using robust fractional PI$^{\lambda}$D controller," *Ain Shams Eng. J.*, vol. 9, no. 1, pp. 77–88, Mar. 2018.

[20] S. R. Kumar, S. Panda, A. Biswal, and G. T. C. Sekhar, "Design and analysis of tilt integral derivative controller with filter for load frequency control of multi-area interconnected power systems," *ISA Trans.*, vol. 61, pp. 251–264, Mar. 2016.

[21] P. Dash, L. C. Saikia, and N. Sinha, "Automatic generation control of multi area thermal system using bat algorithm optimized PD–PID cascade controller," *Int. J. Electr. Power Energy Syst.*, vol. 68, pp. 364–372, Jun. 2015.

[22] M. Raju, L. C. Saikia, and N. Sinha, "Automatic generation control of a multi-area system using ant lion optimizer algorithm based PID plus second order derivative controller," *Int. J. Elect. Power Energy Syst.*, vol. 80, pp. 52–63, Sep. 2016.

[23] A. Daraz, S. Abdullah, H. Mokhlis, I. U. Haq, G. Fareed, and N. N. Mansor, "Fitness dependent optimizer-based automatic generation control of multi-source interconnected power system with non-linearities," *IEEE Access*, vol. 8, pp. 100989–101003, 2020.

[24] M. Ahmed, G. Magdy, M. Khamies, and S. Kamel, "Modified TID controller for load frequency control of a two-area interconnected diverse-unit power system," *Int. J. Electr. Power Energy Syst.*, vol. 135, Feb. 2022, Art. no. 107528.
[25] Y. Arya, "Impact of ultra-capacitor on automatic generation control of electric energy systems using an optimal FFOID controller," *Int. J. Energy Res.*, vol. 43, no. 14, pp. 8765–8778, Aug. 2019.
[26] N. Paliwal, L. Srivastava, and M. Pandit, "Application of grey wolf optimization algorithm for load frequency control in multi-source single area power system," *Evol. Intell.*, vol. 15, no. 1, pp. 563–584, Nov. 2020.
[27] S. P. Ghoshal and S. K. Goswami, "Application of GA based optimal integral gains in fuzzy based active power-frequency control of non-reheat and reheat thermal generating systems," *Electr. Power Syst. Res.*, vol. 67, no. 2, pp. 79–88, Nov. 2003.
[28] P. Aryan, M. Ranjan, and R. Shankar, "Deregulated LFC scheme using equilibrium optimized type-2 fuzzy controller," *WEENTECH Proc. Energy*, vol. 7, no. 1, pp. 494–505, Mar. 2021.
[29] E. M. Ahmed, E. A. Mohamed, A. Elmelegi, M. Aly, and O. Elbaksawi, "Optimum modified fractional order controller for future electric vehicles and renewable energy-based interconnected power systems," *IEEE Access*, vol. 9, pp. 29993–30010, 2021.
[30] B. Khokhar, S. Dahiya, and K. P. S. Parmar, "Atom search optimization based study of frequency deviation response of a hybrid power system," in *Proc. IEEE 9th Power India Int. Conf. (PIICON)*, Feb. 2020, pp. 1–5.
[31] S. A. Taher, M. H. Fini, and S. F. Aliabadi, "Fractional order PID controller design for LFC in electric power systems using imperialist competitive algorithm," *Ain Shams Eng. J.*, vol. 5, no. 1, pp. 121–135, Mar. 2014.
[32] H. S. Salama, G. Magdy, A. Bakeer, and I. Vokony, "Adaptive coordination control strategy of renewable energy sources, hydrogen production unit, and fuel cell for frequency regulation of a hybrid distributed power system," *Protection Control Modern Power Syst.*, vol. 7, no. 1, pp. 1–18, Aug. 2022.
[33] E. A. Mohamed, M. Aly, and M. Watanabe, "New tilt fractional-order integral derivative with fractional filter (TFOIDFF) controller with artificial hummingbird optimizer for LFC in renewable energy power grids," *Mathematics*, vol. 10, no. 16, p. 3006, Aug. 2022.
[34] B. Yang, T. Zhu, X. Zhang, J. Wang, H. Shu, S. Li, T. He, L. Yang, and T. Yu, "Design and implementation of Battery/SMES hybrid energy storage systems used in electric vehicles: A nonlinear robust fractional-order control approach," *Energy*, vol. 191, Jan. 2020, Art. no. 116510.
[35] M. S. Alam, F. S. Al-Ismail, and M. A. Abido, "PV/Wind-integrated low-inertia system frequency control: PSO-optimized fractional-order PI-based SMES approach," *Sustainability*, vol. 13, no. 14, p. 7622, Jul. 2021.
[36] M. Dreidy, H. Mokhlis, and S. Mekhilef, "Inertia response and frequency control techniques for renewable energy sources: A review," *Renew. Sustain. Energy Rev.*, vol. 69, pp. 144–155, Mar. 2017.
[37] A. Fernández-Guillamón, E. Gómez-Lázaro, E. Muljadi, and Á. Molina-García, "Power systems with high renewable energy sources: A review of inertia and frequency control strategies over time," *Renew. Sustain. Energy Rev.*, vol. 115, Nov. 2019, Art. no. 109369.
[38] G. Magdy, G. Shabib, A. A. Elbaset, and Y. Mitani, "Renewable power systems dynamic security using a new coordination of frequency control strategy based on virtual synchronous generator and digital frequency protection," *Int. J. Electr. Power Energy Syst.*, vol. 109, pp. 351–368, Jul. 2019.
[39] E. A. Mohamed, G. Magdy, G. Shabib, A. A. Elbaset, and Y. Mitani, "Frequency stability and digital protection coordination of multi-source power system," *Int. J. Smart Grid Clean Energy*, vol. 7, pp. 240–251, Sep. 2018.
[40] G. Magdy, G. Shabib, A. A. Elbaset, and Y. Mitani, "A novel coordination scheme of virtual inertia control and digital protection for microgrid dynamic security considering high renewable energy penetration," *IET Renew. Power Gener.*, vol. 13, no. 3, pp. 462–474, Jan. 2019.
[41] S. Li, H. Chen, M. Wang, A. A. Heidari, and S. Mirjalili, "Slime mould algorithm: A new method for stochastic optimization," *Future Gener. Comput. Syst.*, vol. 111, pp. 300–323, Oct. 2020.
[42] M. Mostafa, H. Rezk, M. Aly, and E. M. Ahmed, "A new strategy based on slime mould algorithm to extract the optimal model parameters of solar PV panel," *Sustain. Energy Technol. Assessments*, vol. 42, Dec. 2020, Art. no. 100849.
[43] H.-J. Wang, J.-S. Pan, T.-T. Nguyen, and S. Weng, "Distribution network reconfiguration with distributed generation based on parallel slime mould algorithm," *Energy*, vol. 244, Apr. 2022, Art. no. 123011.
[44] Y. Wei, Y. Zhou, Q. Luo, and W. Deng, "Optimal reactive power dispatch using an improved slime mould algorithm," *Energy Rep.*, vol. 7, pp. 8742–8759, Nov. 2021.
[45] T. Kerdphol, M. Watanabe, Y. Mitani, and V. Phunpeng, "Applying virtual inertia control topology to SMES system for frequency stability improvement of low-inertia microgrids driven by high renewables," *Energies*, vol. 12, no. 20, p. 3902, Oct. 2019.
[46] R. J. Abraham, D. Das, and A. Patra, "Automatic generation control of an interconnected hydrothermal power system considering superconducting magnetic energy storage," *Int. J. Electr. Power Energy Syst.*, vol. 29, no. 8, pp. 571–579, Oct. 2007.
[47] S. M. Said, M. Aly, B. Hartmann, A. G. Alharbi, and E. M. Ahmed, "SMES-based fuzzy logic approach for enhancing the reliability of microgrids equipped with PV generators," *IEEE Access*, vol. 7, pp. 92059–92069, 2019.
[48] S. Padhan, R. K. Sahu, and S. Panda, "Automatic generation control with thyristor controlled series compensator including superconducting magnetic energy storage units," *Ain Shams Eng. J.*, vol. 5, no. 3, pp. 759–774, Sep. 2014.
[49] S. M. Said, M. Aly, and H. Balint, "An efficient reactive power dispatch method for hybrid photovoltaic and superconducting magnetic energy storage inverters in utility grids," *IEEE Access*, vol. 8, pp. 183708–183721, 2020.
[50] S. M. Said, E. A. Mohamed, and B. Hartmann, "Coordination strategy for digital frequency relays and energy storage in a low-inertia microgrid," *J. Power Technol.*, vol. 99, no. 4, pp. 254–263, 2020.

EMAD A. MOHAMED received the B.Sc. and M.Sc. degrees in electrical power engineering from Aswan University, Aswan, Egypt, in 2005 and 2013, respectively, and the Ph.D. degree in electrical power engineering from the Kyushu Institute of Technology, Japan, in 2019.

He was a Demonstrator with the Department of Electrical Engineering, Aswan Faculty of Engineering, Aswan University, from November 2007 to August 2013, and an Assistant Lecturer, from 2013 to 2015. He was a Research Student with Kyushu University, Japan, from April to October 2015. He was in a Master Mobility Scholarship at the Faculty of Sciences and Technology, University of Nancy, Lorraine, France. He has been an Assistant Professor at the Faculty of Engineering, Aswan University, since 2019. His current research interests include applications of superconducting power devices, power system control, stability, reliability, and protection.

MOKHTAR ALY (Senior Member, IEEE) received the B.Sc. and M.Sc. degrees in electrical engineering from Aswan University, Aswan, Egypt, in 2007 and 2012, respectively, and the Ph.D. degree from the Department of Electrical Engineering, Faculty of Information Science and Electrical Engineering, Kyushu University, Japan, in 2017.

In 2008, he joined the Department of Electrical Engineering, Aswan University, as an Assistant Lecturer, where he has been an Assistant Professor with the Faculty of Engineering, since 2017. He worked as a Postdoctoral Researcher with the Solar Energy Research Center (SERC-Chile), Universidad Técnica Federico Santa María, Chile, from March 2019 to June 2021. He is currently an Assistant Professor with Universidad San Sebastián, Santiago, Chile. His current research interests include reliability of power electronics systems, especially in renewable energy applications, multi-level inverters, fault tolerant control, electric vehicles, and light emitting diode (LED) lamp drivers. He is a member of the IEEE Power Electronics Society (PELS), the IEEE Industrial Electronics Society (IES), and the IEEE Power and Energy Society (PES).

AHMED ELMELEGI received the B.Sc., M.Sc., and Ph.D. degrees in electrical power engineering from Aswan University, Aswan, Egypt, in 2005, 2019, and 2022, respectively. He joined the Upper Egypt Electricity Distribution Company, Ministry of Electricity and Renewable Energy, Aswan, in 2007. His current research interests include applied power electronics in renewable energy applications, multi-level inverters, and micro-grids.

EMAD M. AHMED (Senior Member, IEEE) received the B.Sc. and M.Sc. degrees from Aswan University, Egypt, in 2001 and 2006, respectively, and the Ph.D. degree from Kyushu University, Japan, in 2012.

He joined the Aswan Power Electronics Applications Research Center (APEARC), from 2012 to 2018. In 2018, he joined the Aswan Wireless Communication Research Center (AWCRC). He is currently working as an Associate Professor with the Department of Electrical Engineering, Faculty of Engineering, Aswan University. Moreover, he is on a leave from the Faculty of Engineering, Jouf University, Saudi Arabia. His current research interests include applied power electronics, especially in renewable energy applications, micro-grids, fault tolerant control, battery management systems, electric vehicles, and LED drivers.

Dr. Ahmed is a member of the IEEE Power Electronics Society (PELS), the IEEE Industrial Electronics Society (IES), and the IEEE Power and Energy Society (PES).

MASAYUKI WATANABE (Member, IEEE) received the B.Sc., M.Sc., and D.Eng. degrees in electrical engineering from Osaka University, Japan, in 2001, 2002, and 2004, respectively. Since 2004, he has been with the Department of Electrical and Electronic Engineering, Kyushu Institute of Technology (Kyutech), Fukuoka, Japan, where he is currently working as a Professor. He is the holder of the PMU Licensed Patent. He has authored numerous books/book chapters and over 200 journals/conference papers. His research interest includes the analysis of power systems.

SAYED M. SAID was born in Aswan, Egypt. He received the B.Sc. and M.Sc. degrees in electrical engineering from Aswan University, in 2006 and 2014, respectively, and the Ph.D. degree from the Doctoral School of Electrical Engineering, Faculty of Electrical Engineering and Informatics, Budapest University of Technology and Economics, Budapest, Hungary. He started to work as a Research Assistant at the Electrical Engineering Department, in 2010. He is currently working as an Assistant Professor at the Electrical Engineering Department, Faculty of Engineering, Aswan University. His research interests include power system analysis, renewable energies, power system control, and wind energy with superconducting magnetic energy storage (SMES). His current research is focused on the integration of wind/PV based on SMES to the utility grids.